AD-A232 127

REPORT DOCUMENTATION PAGE

Form Approved
OMB No. 0704-0188

1. Agency Use Only *(Leave blank).*	2. Report Date. 1988	3. Report Type and Dates Covered. Interim

4. Title and Subtitle.
Biooptical Provinces of the Northeast Pacific Ocear in Summer. A Provisional Analysis Combining Remotely Sensed Ocean Color with Irradiance and Chlorophyll-A Fluorescence Profiles

5. Funding Numbers.
Program Element No. 63704N
Project No. R1299
Task No. 300
Accession No. DN257005

6. Author(s).
J. Mueller and R.E. Lange

7. Performing Organization Name(s) and Address(es).
San Diego State University
Center for Hydro-Optics and Remote Sensing
Sang Diego, CA 92182

8. Performing Organization Report Number.
CR N00014-89-C-6007
N00014-87-C-6002

9. Sponsoring/Monitoring Agency Name(s) and Address(es).
Naval Ocean Research and Development Activity
Code 311
SSc, MS 39529-5004

10. Sponsoring/Monitoring Agency Report Number.

11. Supplementary Notes.

12a. Distribution/Availability Statement.
Approved for public release; distribution is unlimited.

12b. Distribution Code.

13. Abstract *(Maximum 200 words).*

14. Subject Terms.
optics, pacific ocean, ~~physical and dynamic~~ oceanography, biological oceanography

15. Number of Pages. 88

16. Price Code.

17. Security Classification of Report.	18. Security Classification of This Page.	19. Security Classification of Abstract.	20. Limitation of Abstract.
Unclassified	Unclassified		

BIOOPTICAL PROVINCES of the NORTHEAST PACIFIC OCEAN in SUMMER: A PROVISIONAL ANALYSIS COMBINING REMOTELY SENSED OCEAN COLOR with IRRADIANCE and CHLOROPHYLL-A FLUORESCENCE PROFILES.

James L. Mueller

R. Edward Lange

Center for Hydro-Optics and Remote Sensing

San Diego State University

San Diego, CA 92182

ABSTRACT

A provisional biooptical climate of the Northeast Pacific Ocean and Gulf of Alaska in summer combines a regional map of mean remotely sensed K490 (near-surface irradiance attenuation coefficient at 490 nm) with a set of empirical models predicting vertical profiles of irradiance attenuation and in situ chlorophyll-a fluorescence as functions of 1/K490 (m). The K490 seasonal mean was calculated as a composite average of CZCS measurements in this region during June, July and August in 1979 through 1985. Linear regression models on 1/K490 (m) predict depths Z_n (m) at which downwelling irradiance E(Z_n) is n = 10%, 3%, 1%, 0.3% and 0.1% of surface irradiance E(0); separate sets coefficients were derived for optical remote sensing depth ranges 4 < 1/K490 < 20 m and 1/K490 > 20 m, and within each 1/K490 range, from samples of irradiance profiles observed in June-July 1985 and October- November 1982. Vertical profiles of in situ chlorophyll-a fluorescence Fl(z) were available at some stations from each time period; the profile ln[Fl(z)/Fl(z_min)] (where z_min is the depth, below that of the chlorophyll maximum z_max, at which Fl(z) reaches a minimum) is shown to increase linearly with optical depth D(z) = <K(z)>z from the surface to D(z_max), to decrease linearly between D(z_max) and D(z_min), and to remain near zero at z > z_min. Each characteristic profile of fluorescence variation over D(z) may be specified by the four parameters z_max, D(z_min), ln[Fl(0)/Fl(z_min)] (the least-

squares surface intercept), and B_f (the least squares slope between the surface and D(z_max). Regression models are given which allow useful predictions of these parameters, and thereby Fl(z), in three oceanographically distinct biooptical provinces: ECNP central gyre (June-July and Oct-Nov); Gulf of Alaska (July); and California Current System (Oct). Optical and fluorescence profiles measured in and near the North Pacific Subarctic Front were anomalous, indicating it should be classified as a separate biooptical province, but there were too few stations to characterize the dependence of these profile on K490. In the oligotrophic ECNP province, differences between the June/July (1985) and Oct/Nov (1982) optical attenuation and fluorescence profile models are consistent with a weakening of the fluorescence maximum over time, which may be due to progressive nutrient depletion in the euphotic zone during the period of shallow mixed layer stratification between the spring transition (in April or May) and when the mixed layer deepens into the nutricline in the fall transition (November-December); this finding should pose a useful working hypothesis for future research. The vertical profile models are applied to the summer mean CZCS K490 to describe meridional (near 150W) and zonal (near 32N) profiles of light attenuation with depth, and of the depth and strength of the chlorophyll-a fluorescence maximum.

LIST of SYMBOLS and ACRONYMS

AG	Alaskan Gyre, the biooptical water masses associated with circulation within the Gulf of Alaska, but not including areas influenced by the SAF near 42N (which appear to be biooptically distinct).
CCS	California Current System, biooptical water masses of which are assumed to include both eutrophic water masses over the continental slope and shelf, and mesotrophic water masses occupying the transition into the ECNP central gyre.
CZCS	The Nimbus-7 Coastal Zone Color Scanner, a multispectral ocean color radiometer which measured images of spectral radiance upwelled from the ocean and atmosphere at wavelengths of 443, 520, 550 and 670 nm.
D(z)	Diffuse Optical Depth at depth z $D(z) = \langle K(z) \rangle z$ Wavelength is 490 nm unless specified.
ECNP	East Central North Pacific (used with reference to oligotrophic water masses of the central gyre).

E(z)	Downwelling irradiance at depth z. Wavelength is 490 nm unless specified.
Fl(z)	Chlorophyll-a fluorescence (in volts) measured in situ at depth z.
K(z)	Diffuse irradiance attenuation coefficient at depth z. Wavelength is 490 nm unless specified.
K490	Mean irradiance attenuation coefficient at 490 nm to depth z = 1/<K(490,z)>, i.e. the mean value over the top optical depth D(1/K490) = 1.0. The symbol is used without parentheses to distinguish its reference to the value of "surface K(490)" estimated from remotely sensed ocean color.
<K(z)>	Mean irradiance attenuation coefficient from the surface to depth z, for wavelength of 490 nm unless specified.
STF	The North Pacific Subtropical Front, a persistent zonal feature of the NE Pacific ocean circulation maintained by Ekman convergence near 33N.

z	Depth (m) below the sea surface.
z_max	Depth (m) of the in situ chlorophyll-a fluorescence maximum.
z_min	Depth (m) of the deep background minimum in chlorophyll-a fluorescence.
Z_n	Depth (m) at which E(Z_n) is attenuated to n% of incident surface irradiance E(0).

INTRODUCTION

Remotely sensed ocean color can be used to determine phytoplankton pigment concentrations and optical diffuse attenuation coefficient K(490) in the near-surface layer of the ocean. Regional and global distributions of these biooptical variables have been successfully produced in a variety of experiments, using data measured with the Nimbus-7 CZCS. The CZCS has been described by Hovis, et al. (1980).

An often voiced concern is that remotely sensed biooptical properties represent only a shallow surface layer of the sea, and provide no direct information on important features in the vertical profiles of chlorophyll and optical properties. For example, maxima in vertical profiles of chlorophyll-a concentrations (and chlorophyll-a fluorescence) are typically found at depths 2 to 3 times deeper than that probed by passive ocean color measurements, and the values at the maxima may be several times larger than those near the surface. This characteristic profile shape has frustrated attempts to correlate surface measured chlorophyll-a concentrations with concentrations integrated through the euphotic zone in oligotrophic waters (Hayward and Venrick, 1982), and CZCS pigment biomass estimates were found to be poorly correlated with vertically integrated values in a persistent eddy off the California Coast (Haury, et

al., 1986). On the other hand, unpublished analyses of K(490, z) profiles at the Scripps Visibility Laboratory showed statistically significant correlations between CZCS K490 and the mean attenuation coefficient to 100 m <K(490 nm, 100m)> (R.W. Austin, SIO Visibility Lab., La Jolla, CA, personal communication, 1984).

In this paper we report a set of regression models, applicable to the Northeast Pacific ocean, which predict the vertical profiles of both diffuse optical depth (490 nm) and normalized chlorophyll-a fluorescence from a single variable which may be estimated from remotely sensed ocean color: optical remote sensing depth 1/K490 (m). Following an approach first suggested by Platt and Sathyendranath (1988), the analysis is organized within "biooptical provinces", which partition the study region geographically, and by time of year within each province.

The in-water profile models are applied to a composite summer (June-August) mean CZCS K490 distribution, prepared provisionally as a guide for classification of biooptical provinces and as a working framework for preliminary analyses of combined CZCS and in situ biooptical data. The present work is an entirely empirical description of systematic interrelationships (and temporal trends) between vertical profiles of biooptical variables and remotely sensed ocean color. Such descriptions can serve as operationally useful biooptical predictors in their own right, and in the longer term may support development and

validation of predictions through theoretically based simulations of physiological response of phytoplankton populations to physical and radiative forcing within biooptical provinces.

For purposes of the present analysis, the Northeastern Pacific region is partitioned geographically into the 4 biooptical provinces illustrated in Fig. 1 (heavy dashed lines), which are associated with well known features of the regional ocean circulation:

1) CCS: The currents and water masses of the California Current System. In the present analysis, the western boundary of the CCS province is identified with the transition from low salinity water masses (of subarctic origin) to higher salinity water masses of the ECNP central gyre near 130W; this boundary is not necessarily distinguishable in remote sensing imagery and must be located from concurrent or climatological temperature and salinity data.
2) ECNP: The oligotrophic water masses of the East Central North Pacific central gyre. The province is bounded on the north by the SAF and in the east by the CCS province. The zonal dotted line marked "STF" marks the approximate location of the subtropical front near 33N, which corresponds to the southern limit of the climatological zone of convergence in Ekman transport extending southward from the SAF near 42N (Roden, 1975); the

Temperature/Salinity curves of ECNP water masses on either side of the STF can be used to segregate "north" and "south" varieties of ECNP water (Niiler and Reynolds, 1984).

3) SAF: The Eastern North Pacific Subarctic Front is a zonal convergence feature, usually found between 42N and 45N, which is characterized by compensating horizontal gradients of temperature and salinity, and therefore weak horizontal density gradients, in the upper 100 m and moderate horizontal density gradients below 100m (Roden, 1975, 1977). Biooptically, the surface layer in the front appears as a ridge of high chlorophyll and particle concentration (and thus low optical remote sensing depth 1/K490), decreasing sharply into the ECNP province to the south, and decreasing slightly into the more patchy distribution of turbidity associated with the Alaskan Gyre (AG) to the north and east (Pak, et al., 1988; and present results below).

4) AG: The Alaskan Gyre, comprising the currents and water masses in the Gulf of Alaska.

The above association of biooptical provinces with ocean current regimes differs slightly from the approach of Platt and Sathyendranath (1988), who organized the North Atlantic (between 20N and 50N) into nine regions based on depth (shelf, slope and oceanic) and latitude (equatorial, subtropical, and

transitional), with the subtropical/transitional boundary fixed by inspection of the satellite imagery. They approached biooptical characterization of water masses by assuming that within a province in a given season, the vertical profile over depth of pigment biomass is stable in shape, that the shape can be approximated by a Gaussian function, and that its parameters remain "quasi-constant". The present, slightly different, approach to biooptical characterization of provinces is based on a conceptual "equilibrium model" of optical depth and fluorescence (Fig. 2) which evolves from three assumptions:

1) the deep minimum fluorescence Fl(z_min) found below the euphotic zone (Fig. 2a) is a "background fluorescence" which may be treated as a linear sensitivity measure of an individual fluorometer, so that when normalized by this value, profiles measured with different fluoremeters may be treated as equivalent;
2) within a given province and period of several weeks, light adaptation by the phytoplankton population will tend to establish a "log-linear equilibrium profile" of chlorophyll-a fluorescence over diffuse optical depth D(z) (indexed at 490 nm), and an associated equilibrium profile in D(z) (Fig. 2b and 2c); and
3) within a given province and time period, systematic variation over geographic distance in the associated equilibrium profiles of fluorescence and diffuse optical depth is the primary cause of horizontal variability in

optical remote sensing depth 1/K490 (which represents the upper "tail" of the optical depth profile).

If these assumptions are valid, significant correlations should exist (within provinces and time periods) between 1/K490 and characteristic parameters of the optical depth and chlorophyll-a fluorescence profiles.

The conceptual model of equilibrium fluorescence profiles is illustrated by the three curves of Fig. 2. The vertical profile of in situ chlorophyll flourescence Fl(z)/Fl(z_min) is shown in Fig. 2a, normalized to the deep background minimum flourescence at depth z_min. A subtlety illustrated in Fig. 2a is that surface fluorescence may be less than Fl(z_min). The curve in Fig. 2b illustrates the vertical profile over depth z (m) of diffuse optical depth D(z), which may be calculated directly from a measured vertical profile of downwelling irradiance E(z). [D(z) is the mirror image of a logarithmic plot of irradiance, normalized by E(0) over depth.] To analyse data from a single station, the log-linear equilibrium profile (2c) is determined by a least squares fit to paired profiles ln[Fl(z)/Fl(z_min)] vs D(z) calculated from measured Fl(z) and E(z) profiles respectively. From samples of fitted station data representing a given biooptical province and time, regression equations are determined relating 1/K490 to characteristic parameters of D(z) (2b) and the equilibribum profile (2c) To predict biooptical profiles from 1/K490, the regression equations for a

province/time are employed to predict curves 2b and 2c, which are then combined to construct profile 2a.

DATA and METHODS of ANALYSIS

Vertical profiles over depth of downwelling irradiance at 490 nm E(z) were extracted from the data reports of four separate cruises in the Northeast Pacific Ocean (Fig. 1 cruise tracks). Accompanying profiles of chlorophyll-a fluorescence Fl(z) were also measured during two of these cruises. In October-November 1982, E(z) and Fl(z) data were acquired aboard the R/V Acania in CCS and ECNP water masses near 34N (Fig. 1, track "A"), (Smith, R.C. and K.S. Baker, Optical Dynamics Experiment (ODEX) III Cruise, 10 October - 17 November 1982, Vol. 5: BOPS Vertical Cast Measurements, SIO Ref. 87-23, Sept. 1987). Also during Oct.-Nov. 1982, E(z) profiles were measured aboard the R/V DeSteiguer at stations distributied along a trackline from San Diego westward into the CCS to (30N, 142W), thence northwest to the SAF near (45N, 145W), and returning from there to San Diego (Fig. 1, track "B"; SIO VisLab TM:DL-001-83t, 22 Feb. 1983: Optical Data from USNS De Steiguer SLC Cruise 26 Oct. - 15 Nov. 1982). In June 1985, additional E(z) profiles were measured aboard the R/V DeSteiguer along a cruise track from Seattle to and from the Bering Sea through the AG (Fig. 1, track "C"; SIO VisLab TM:EN-009-85t, 10 July 1985: Measured Optical Properties of Ocean Water: USNS DeSteiguer, North Pacific and Bering Sea, 5 June - 25 June 1985). Finally in June-July 1985, E(z) and Fl(z) profiles were measured aboard the R/V Discoverer on a transect near 150W

from Hawaii through the ECNP, SAF and AG provinces to Kodiak (Fig. 1, track "D"; OSU Optical Oceanography Group Cruise Data Report, R/V Discoverer 28 June - 23 July 1985), results of which have been reported by Pak, et al. (1988).

The in situ profiles were first screened for quality. Data from stations were rejected for the following reasons:

1. If the local solar zenith angle was greater than 60 degrees.
2. If incident surface irradiance measured by a deck radiometer (when available) varied by more than a few percent during a cast.
3. If temperature or salinity inversions in an accompanying CTD profile (when available), suggested lateral mixing or interleaving of distinctly different water masses across fronts, which would break up any equilibrium profile characteristics.
4. If a vertical profile Fl(z) did not extend from the surface to a depth z_min where a deep background fluorescence minimum was observed.

The remaining irradiance and fluorescence profiles were organized into two subsamples of stations occupied within two separate two-month periods (June-July 1985 and October-November 1982). We henceforth refer to these as "Jun/Jul" and "Oct/Nov" subsamples respectively. For profiles from each period, preliminary scattergrams were used to reveal visual correlations

between optical remote sensing depth 1/K490 and characteristic parameters of the vertical irradiance and chlorophyll-a fluorescence profiles. These preliminary scattergrams were also examined to partition the data from each period into subsets associated with geographically distinct biooptical provinces (Fig. 1), with possible further partitioning by magnitude of 1/K490.

Irradiance Profile Analysis

From each vertical profile of spectral irradiance E(z) (at 490 nm), the vertical profile of diffuse optical depth was calculated as

$$D(z) = \ln[\, E(0) \,/\, E(z) \,]. \qquad (1)$$

From the D(z) profile, the optical remote sensing depth 1/K490 was determined as the depth (m) where D(1/K490) = 1.0, i.e. the depth at which E(z) = E(0) exp(-1) [or 37% of surface irradiance]. Depths Z_n (m) at which E(Z_n) = 10%, 3%, 1%, 0.3% and 0.1% of E(0) were extracted from each irradiance profile at optical depths D(Z_n) = 2.30, 3.51, 4.61, 5.81 and 6.91 respectively.

Variations in each light attenuation depth Z_n over varying 1/K490 were examined separately within each subsample. At each Z_n, statistically significant regression relationships of the form

$$Z_n = A_n + B_n / K490, \qquad (2)$$

were determined, with four separate families of coefficients for two optical remote sensing depth ranges (1/K490 < 20 m and and 1/K490 > 20 m) within Jun/Jul and Oct/Nov (Figs. 3 - 5).

Chlorophyll-a Fluorescence Profile Analysis

Vertical profiles of in situ chlorophyll-a fluorescence Fl(z) (in volts) were normalized as Fl(z)/Fl(z_min), where Fl(z_min) is the deep background minimum (Fig. 2a). The measured values ln[Fl(z)/Fl(z_min)] and D(z) were then paired at each depth z (from the surface to z_min) to create a discrete represenatation of the log-linear equilibrium fluorescence profile (Fig. 2c). Simple linear regression analysis was used to fit the upper segment of the measured data (0 to z_max) to the log-linear equilibrium profile as

$$\ln[Fl(z)/Fl(z\_min)] = \ln[Fl(0)/Fl(z\_min)] + B\_f * D(z); \qquad z < z\_max. \qquad (3)$$

A second least-squares fit of ln[Fl(z)/Fl(z_min)], D(z) pairs between z_max and z_min was used to determine the lower intercept D(z_min) (the diffuse optical depth of the deep minimum "background" fluorescence), such that

$$\ln[Fl(z)/Fl(z\_min)] = \ln[Fl(z\_max)/Fl(z\_min)] * [\, D(z\_min) - D(z) \,] / [\, D(z\_min) - D(z\_max) \,] ; \quad z\_max < z < z\_min. \qquad (4)$$

In this approach, each vertical chlorophyll-a fluorescence profile is approximated through equations (3) and (4) by four characteristic parameters z_max (depth in meters of the chlorophyll fluorescence maximum), ln[Fl(0)/Fl(z_min)] (fitted surface fluorescence), B_f (least squares slope of increasing fluorescence with optical depth between the surface and z_max), and D(z_min) (the diffuse optical depth of the minimum "background" fluorescence). The optical depth D(z_max) of the chlorophyll-a fluorescence maximum is determined from the accompanying optical depth profile model given z_max. The decision to parametrize fluorescence profiles with these four particular quantities is entirely retrospective: these variables were found to be better correlated with some function of remote sensing K490 than were the alternative choices.

Another set of scatter diagrams was prepared to identify exploitable correlations between either optical remote sensing depth 1/K490, or [K490 - 0.02] [where 0.02 is the approximate value of K(490) for pure water] and each of the above four parameters of the Fl(z)/Fl(z_min) profile within otherwise distinguishable biooptical provinces. Separate relationships were identified within: 1) ECNP (central gyre Jun/Jul and

Oct/Nov), 2) AG (July 1985 only), and 3) CCS (October 1982 only).

The depth of the chlorophyll-a fluorescence maximum is predicted from the regression equation

$$\ln[\ z\_max\ ] = A\_c + B\_c \ln[\ 1/K490\ ], \qquad (5)$$

where the coefficients A_c and B_c vary between the Jun/Jul and Oct/Nov samples, but do not vary geographically (Fig. 8).

Diffuse optical depth of the deep fluorescence minimum is predicted from the regression equation

$$\ln[D(z\_min)] = A\_m + B\_m \ln[\ K490 - 0.02\ ], \qquad (6)$$

where the coefficients A_m and B_m vary between the Jun/Jul and Oct/Nov samples, but not geographically (Fig. 9).

The surface intercept of the log-linear equilibrium fluorescence profile is predicted from the regression equation

$$\ln[Fl(0)/Fl(z\_min)] = A\_o + B\_o \ln[\ K490 - 0.02\ ], \qquad (7)$$

where coefficients A_o and B_o vary both with time of year and geographic (water mass) biooptical province (Fig. 10).

Finally, the slope of the fluorescence profile over optical depth is predicted from the regression equation

$$B\_f = A\_z + B\_z \ln[\ K490 - 0.02], \qquad (8)$$

where coefficients A_z and B_z also vary both with time of year and with geographic (water mass) biooptical province (Fig. 11).

Nimbus-7 CZCS K490 Analysis

A complete set of Nimbus-7 CZCS level-1 (earth located radiance counts) data files covering the Northeast Pacific region were copied from the SIO Visibility Laboratory tape archive (which was transferred to the SIO Remote Sensing Facility following the disestablishment of the Visibility Laboratory) onto digital VHS cassettes (each with a capacity of approximately 150 CZCS 2-minute image files). The portion of this data set spanning the months of June, July and August in years 1979 through 1985 was processed to produce a composite mean CZCS remotely sensed K490 distribution as a provisional working framework within which to begin developing a spatial and temporal biooptical province classification of the Northeast Pacific.

A composite average map of K490 in the NE Pacific was prepared from all CZCS data acquired during summer months (June - August) over 7 years (1979 - 1985). Each individual image was screened to eliminate areas either contaminated by sun glint or totally covered by land or clouds, and to determine the wavelength dependence of aerosol radiance when suitable "clear-water" pixels were present in a scene (Gordon and Clark, 1981). Atmospheric correction algorithms are described by Gordon, et al. (1983), with the Mueller (1985) model used to reduce the CZCS calibration sensitivity over time. CZCS observations of open-water areas immediately to the right of clouds, which may be contaminated by

electronic overshoot, were eliminated from each scan line (Mueller, 1988). K490 was calculated at each valid open-water pixel using the algorithm of Austin and Petzold (1981), which they recently reconfirmed using a larger and more geographically diverse optical data set than was originally available (R. W. Austin, Scripps Institution of Oceanography, personal communication 1989).

Individual CZCS K490 estimates were inserted into daily map files (a Mercator grid with 5 km resolution) at the proper geographic location using a "nearest neighbor" resampling algorithm. Each daily K490 map was then displayed and inspected for quality. A small fraction (< 5%) of the CZCS data were rejected at this stage, either due to obvious geolocation errors or to anomalies in K490 patterns or magnitudes which suggested symptoms of possible discrepancies in radiometric or algorithmic performance. The remaining daily maps were combined to form monthly composite means for each June, July and August of each year. The monthly composite means (and associated sample sizes) were combined to form June, July and August composite grand means over the 7 years of CZCS coverage (1979 thru 1985). And finally the three monthly composite grand means were combined, in turn, to form the provisional summer composite mean CZCS K490 (Fig. 15 below).

The CZCS K490 seasonal average presented in this paper is no better than a semi-quantitative estimate of the biooptical climate of the region. In the early phases of the analyses

reported here, it quickly emerged that at least a "first-guess" example of a CZCS seasonal mean was urgently needed as a basis for organizing the research. A reasonably complete spatial coverage of the summer mean patterns of K490 was required to guide a geographic partition of the region into biooptical provinces, and a summer example of a seasonal CZCS K490 mean would allow preliminary comparisons to be made between the CZCS and in situ biooptical data.

The most critical deficiency of the provisional CZCS mean stems from the use, in its preparation, of a linear single scattering approximation of Rayleigh radiance for atmospheric corrections (Gordon, et al., 1983), rather than the now accepted standard multiple scattering Rayleigh radiance model of Gordon, et al. (1988). The errors due to this approximation alone are only a few percent when solar zenith angles remain less than 45 degrees, and it is generally agreed that an internally consistent application of either of the two atmospheric correction models will yield comparable estimates of phytoplankton pigment concentrations and K490 under these restricted conditions (Gordon, et al., 1988). In either approach, an "internally consistent" analysis demands a proper evaluation of the time dependent changes in the radiometric sensitivity of the CZCS (Gordon, et al. 1983; Mueller, 1985; Gordon, et al. 1988), which must be carried out within the framework of whichever atmospheric correction algorithm is employed.

RESULTS

Irradiance Attenuation Profile Analyses

Regression lines relating optical remote sensing depth 1/K490 (m) to depths Z_n (m) where irradiance E(z) is attenuated to 10%, 3%, 1%, 0.3% and 0.1% of E(0) (bottom to top dashed lines respectively) are illustrated in Fig. 3 for Jun/Jul stations in the ECNP central gyre ("o") and AG ("*"). Stations from the Bering Sea and SAF (near 42N), and cases where 1/K490 < 4 m (which occurred only in, or very near, water depths < 200m) were excluded from the regression analysis. The scatter in measured (1/K490, Z_n) about the regression lines is illustrated only for the Z_10%, Z_1% and Z_0.1% irradiance attenuation depths. (Scatter at Z_3% and Z_0.3% are similar, but are not shown to avoid cluttering the figure). Z_n are strongly correlated with 1/K490 over the entire range of observations, but the slopes of the regressions are obviously much steeper in the range 1/K490 < 20, than in the range 1/K490 > 20 m. We therefore determined a separate family of regression lines [equation (2)] for the five Z_n depths in each 1/K490 range [4 m < 1/K490 < 20 m, and 1/K490 > 20 m].

Regression lines, and associated scatter, of Z_n versus 1/K90 for E(z) profiles observed at Oct/Nov stations in the ECNP central

gyre ("o) and AG ("+") are illutrasted in Fig. 4 in a format identical to that of Fig. 3. Again, the five sets of (dash -- dash) lines, from bottom to top resepectively, predict at each 1/K490 (m) the depths Z_n (m) at which E(Z_n) are 10%, 3%, 1%, 0.3% and 0.1% of E(0), with scatter of observations about the regression shown only for Z_10%, Z_1% and Z_0.1% depths. As in the Jun/Jul case, the Oct/Nov Z_n are strongly correlated with 1/K490, with distinctly different slopes in the ranges of 1/K490 below and above 20 m. In the Oct/Nov subsample however, the break in slope near 1/K490 = 20 m is considerably weaker than that seen in the Jun/Jul scattergrams of Fig. 3 (in Fig. 4, the break effectively disappears below the 1% light level).

Table 1 contains a list of regression coefficients A_n and B_n to be used in equation (2) to calculate Z_n at each n% light level. Separate sets of coefficients for Jun/Jul (Fig. 3) and Oct/Nov (Fig. 4) are listed for each range of optical remote sensing depth [1/K490 < 20 m and 1/K490 > 20 m]. The two sets of coefficients for 1/K490 > 20 m represent a common geographic water mass regime (ECNP), but the same is not true for 1/K490 < 20 m coefficients: the Jun/Jul set represents profiles in the AG and the Oct/Nov set represents profiles in the CCS. The number in parentheses beside each A_n and B_n value in Table 1 is its 95% confidence limit. Also listed are the squared correlation coefficient (r*r) and residual standard deviation (S_xy) about the regression line for each case; based on Fisher's F

distribution, all regression results in Table 1 are significant at the 0.995 level, and the data are well distributed over the range of the fit (see Figs. 3 and 4).

In Fig. 5 we compare the four families of Z_n vs 1/K490 regression models from Figs. 3 and 4 for June-July (1985) and October-November (1982) respectively. In the range of 1/K490 > 20 m, the slopes of regression lines for both time periods are dominated by the transparency of the oligotrophic water masses of the ECNP central gyre. The slopes of the October-November (1982) lines are steeper than the those of the June-July (1982) model primarily because ECNP water was more transpaent at the beginning of the fall transition (Oct-Nov) than in mid-summer (June-July). It is probably reasonable to attribute these differences to a within-summer temporal trend, even though the data were acquired in different years. It would be far less reasonable to interpret the differences in the comparison of regression lines in the range 1/K490 < 20 m as a temporal tendency between June-July and October-November. In this "eutrophic" range of 1/K490, the Fig. 3 (June-July 1985) regression lines (dash curves) characterize variations in the vertical light attenuation profile in the AG during mid-summer. The Fig. 4 (October-November 1982) regression lines (dash--dash curves), on the other hand, characterize variations in the vertical light attenuation profile in the CCS at the end of a full season of coastal upwelling.

Comparing first the coefficients (and 95% confidence limits)

between the two time periods within the range 1/K490 < 20 m, the Z_10% coefficients are not significantly different, the Z_3% coefficients are nearly parallel (Fig. 5) with significantly separated intercepts, and the Z_1% through Z_0.1% coefficients are all statistically different. Comparing the two time periods within the oligotrophic 1/K490 > 20 m range (Fig. 5), the Z_10% and Z_3% regressions are parallel but sigificantly separated (by 10 m), and the Z_1% and deeper coefficients are all significantly different.

Within the Jun/Jul period, the regression equations at each Z_n for 1/K490 < 20 m are significantly different from those for 1/K490 > 20 m (with the possible exception of the Z_10% equation). Within the October-November (1985) period, the Z_10% and Z_3% equations are significantly different in the two 1/K490 ranges, but at the 1%, 0.3% and 0.1% light levels the coefficients are not significantly separated and one could argue for a single regression fit over the entire 1/K490 range.

In the Jun/Jul oligotrophic 1/K490 > 20 m regression family, the slopes B_n are effectively parallel at all levels between Z_3% and Z_0.1% (Bn = 2.0 approximately), and B_10% falls barely outside the 95% confidence limits of the deeper coefficients. In the remaining cases, the slopes B_n increase monotonically from the 10% to the 0.1% light levels and their 95% confidence limits are well separated.

To calculate a modeled optical depth profile D(z) given 1/K490, the appropriate coefficients are selected from Table 1 and substituted in equation (2) to calculate the sequence of 7 attenuation depths 0, 1/K490, Z_10%, ..., Z_0.1% m corresponding the the 7 optical depths 0, 1.0, D(Z_10%), ..., D(Z_0.1%). For depths z < Z_0.1%, D(z) is determined by linear interpolation. For depths z > Z_0.1%, optical depth is extrapolated as

$$D(z) = 6.91 + 1.2\,[z - Z_{0.1\%}] / [Z_{0.1\%} - Z_{0.3\%}].$$

In Fig. 6, attenuation depths Z_n for the n = 10%, 1% and 0.1% irradiance levels from four E(z) profiles measured in the Bering Sea during June 1985 are superimposed (symbol "d") on the respective Z_n vs 1/K490 regression lines (Fig. 3). Clearly these optical profile characteristics are well matched by the regression fit to profiles observed in the AG during the same approximate time period.

In Fig. 7, the scatter of depths Z_n at which E(Z_n) were 10%, 1% and 0.1% of E(0) in irradiance profiles from stations in the SAF (between 40N and 44N near 150W) in Jun/Jul ("x") and Oct/Nov ("X") are compared with the corresponding regression lines of Fig. 3. Attenuation depths Z_10% (and Z_3% - not shown) in the SAF profiles agree reasonably with the Jun/Jul regression prediction on 1/K490, but Z_1% through Z_0.1% become progressively much deeper than the model would predict at the observed 1/K490. The mean depth interval Z_0.1% - Z_1% is 74 m (for the four SAF profiles which extend that deep), which is

equivalent to a constant K(z) = 0.03 (m**-1). To model irradiance attenuation profiles for stations in the SAF, we will use a value halfway between 0.03 and the effective K for the Z_10% < z < Z_3% interval to estimate Z_1%, and extrapolate optical depths below the 1% level using K = 0.03 (m**-1).

Chlorophyll-a Fluorescence Profile Analysis

Chlorophyll-a fluorescence profiles were measured in situ at 19 of the biooptical stations in the ECNP and AG Jun/Jul subsample and 33 stations in the ECNP and CCS Oct/Nov subsample. Each profile was normalized as ln[Fl(z)/Fl(z_min)] and paired with optical depth D(z) calculated from the accompanying E(z) profile. With increasing depth below z_min in all profiles, Fl(z) remained constant within a few percent of Fl(z_min) [consistent with the assumed model construct of Fig. 2a]. A log-linear equilibrium fluorescence profile (of the form illustrated in Fig. 2c) was estimated for each station by linear regression fits to the upper [D(0) to D(z_max)] and lower [D(z_max) to D(z_min)] segments of each ln(Fl[D(z)]/Fl(z_min)) profile. An excellent fit was obtained between ln[Fl(z)/Fl(z_min)] and D(z) for every station examined: squared correlation coefficients for the fit to the top (bottom) profile segments exceeded 0.70 in 100% (100%), 0.80 in 97% (96%), 0.90 in 86% (85%), and 0.95 in 62% (55%) of the casts.

The four parameters z_max, ln[Fl(0)/Fl(z_min)], B_f and D(z_min) were determined from the log-linear equilibrium profile fits and

plotted in scatter diagrams to reveal systematic dependencies on remotely sensed K490 within provinces and time periods. The following general observations were used to qualitatively characterize the provinces and subdivide the data for regression analyses:

The trends in z_max with increasing 1/K490, and in D(z_min) with [K490 - 0.02], appeared to be continuous across provinces within Jun/Jul (ECNP, SAF and AG) and Oct/Nov (ECNP and CCS-Oct), with only the four CCS-Nov profiles displaying anomalous scatter.

The slope B_f and surface intercept ln[Fl(0)/Fl(z_min)] of the upper segment of the log-linear equilibrium fluorescence profile (Fig. 2c), together proved to be the strongest discriminant of differences in biooptical profile characteristics in different geographic provinces. The SAF (Jun/Jul) and CCS-Nov values of B_f and ln[Fl(0)/Fl(z_min)] were anomalous with respect to the other observations in their time periods and there were too few stations to pursue separate analyses in either province (they were simply excluded from the regressions). With data from these provinces excluded, the scatter in each these parameters, plotted against 1/K490, showed distinctly different tendencies at the extremes in 1/K490 characteristic of each province (1/K490 < 20m in AG and CCS, and 1/K490 > 30 m in ECNP), but merged into enormous confusion in the intermediate

range of 1/K490 between 20 and 30 m which occurs in water masses within all three provinces. In Jun/Jul data, the SAF serves as a geographic buffer, which is readily detectable in the remotely sensed K490 (or pigment biomass) imagery, between the AG and ECNP provinces; when the data were separated on this basis, exploitable tendencies between both parameters and [K490 - 0.02] were apparent in each province. In the Oct/Nov subsample, on the other hand, a reasonable boundary between ECNP and CCS provinces could not be determined on the basis of optical remote sensing depth 1/K490 alone. With recourse to temperature and salinity data from transects across the CCS and into ECNP in Oct/Nov 1982 [Fig. 1, track A; Stockel, J.A., et al. 1986. Data from the Optical Dynamics Experiment (ODEX) R/V Acania Expedition of 10 Oct - 17 Nov 1982. Vol 1: CTD and Optics Profiles, Naval Postgraduate School data report NPS-68-86-013], October 1983, and April 1984 (unpublished data in our possession), the western boundary of the CCS province was placed at approximately 34N, 130W to coincide with the transition from low salinity water masses (of subarctic origin) to higher salinity water masses within ECNP. The CCS-ECNP boundary (Fig. 1) was then sketched through this location to generally parallel the coastline and the trend in offshore K490 gradients observed in the CZCS K490 mean (Fig. 15 below). With geographic discrimination of ECNP Oct/Nov and CCS-Oct, distinctly different dependencies on K490 of B_f and

ln[Fl(0)/Fl(z_min)] became visually apparent in each province.

The best predictions of z_max were obtained with 1/K490 in the log-linear form of equation (5), with separate coefficients A_c and B_c for Jun/Jul and Oct/Nov. The scatter of z_max vs 1/K490 observations from these two time periods are illustrated in Figs. 8a and 8b respectively, together with the linear regression lines for each subsample. Coefficients A_c and B_c are listed in Table 2, with squared correlation coefficients and residual standard deviations; the Fisher's F test shows both regressions to be statistically significant at the 0.995 level, and the 95% confidence limits of the respective regression coefficients do not overlap. The Jun/Jul subsample (Fig. 8a) includes observations from the AG (*), SAF (x) and ECNP (o), with all data points included in the regression fit. The Oct/Nov subsample (Fig. 8b) includes observations from ECNP (o), CCS-Oct (+) and CCS-Nov (#; points excluded from the regression fit); the four CCS-Nov (#) profiles were observed at two adjacent, nearshore stations on 17 November 1982 and are clearly anomalous with respect to the more widely distributed CCS-Oct (+) stations observed four weeks earlier.

The optical depth of the deep fluorescence minimum D(z_min) was best predicted by equation (6) as a log-linear function of [K490-0.02] , where 0.02 m**-1 is approximately the diffuse attenuation coefficient of pure water. Scatter of ln[D(z_min)]

with ln[K490-0.02] is graphed in Figs. 9a and 9b for the Jun/Jul and Oct/Nov subsamples respectively. The regression fit for Jun/Jul (Fig. 9a; dash line) is based on data from the AG (*), SAF (x) and ECNP (o). The regression fit for Oct/Nov (Fig. 9b; dash--dash line) is based on data from the CCS-Oct (+), CCS-Nov (+) and ECNP (o). Coefficients A_m and B_m for the two regression equations are given in Table 2; the two equations are statistically different, and F-tests show both to be significant at the 0.995 level (despite the low squared correlation coefficient of 0.38 for the Jun/Jul regression).

The surface intercept of the fluorescence profile, ln[Fl(0)/Fl(z)], is predicted by equation (7) as a function of ln[K490 - 0.02]. Regression fits and associated scatter are illustrated in Fig. 10a for CCS-Oct (+; solid line) and AG Jun/Jul (*; dash-dot-dash line). The fit to CCS-Oct data is excellent (r*r = 0.93, the data are well distributed over the range of the fit, and the associated F statistic is significant at the 0.995 level). The regression fit to the Jun/Jul AG data is only significant at the 0.95 level, and its slope is dominated by the two extreme values at the upper right of the scattergram. The CCS_Nov data (#) are scattered widely between the two regression lines, and don't appear to be associated with either regression sample.

Surface fluorescence intercepts ln[Fl(0)/Fl(z_min)] for ECNP Jun/Jul (x; dash line) and Oct/Nov (o; dash--dash line), along

with separate regression lines for each time period (having excluded one apparently obvious outlier from each subsample) are illustrated in Fig. 10b. Coefficients A_o and B_o, for predicting ln[Fl(0)/Fl(z_min)] with equation (7), are given in Table 2 for each time period. The Oct/Nov equation (despite a low r*r = 0.44) is significant at the 0.995 level, but by itself (because of the extremely small sample size), the F statistic of the Jun/Jul regression is not statistically significant at even the 0.90 level. On the other hand, the slope coefficients B_o are practically identical for the two samples. Were an alternate regression model assumed, to use the Oct/Nov slope B_o and fit only the shifted intercept A_o to the 5 Jun/Jul data points, that regression would be significant at the 0.90 level. And from a purely pragmatic viewpoint, the construct of temporally shifting parallel dependency of the surface intercept on ln[K490 - 0.02] appears to better reproduce variability in the ECNP deep fluorescence maximum than do other interpretations of this data.

Before adopting the separate (parallel) ln[Fl(0)/Fl(z_min)] regression models shown, a single regression fit was attempted through the combined ECNP sample illustrated in Fig. 10b. Taken by itself at face value, the linear fit to the combined sample was statistically better than either of the models shown here. In initial experiments with fluorescence profile reconstruction, however, the profile model's representation of variation the ECNP deep chlorophyll maximum with varying K490 was found to be very

sensitive to small variations in the surface intercept, given a between time-periods shift in slope B_f. In the ECNP province, B_f exhibits no significant dependence on K490 and remains essentially constant within each two-month period (see below). When the steeper slope of the overall (combined sample) surface intercept model interacted with the mean slopes B_f, the deep chlorophyll maxima in most of the observed ECNP fluorescence profiles were not well represented by the model. A second formulation, using the mean value of surface intercept from each time period with its associated mean, yielded a slight qualitative improvement in Fl(z)/Fl(z_min) profile prediction. Finally however, the separate parallel models for surface intercept dependence on K490 in the two time periods (Fig. 10b and Table 2) were determined to yield the most reasonable reproduction of variations in the observed ECNP fluorescence profiles.

The slope B_f of increasing ln[Fl(z)/Fl(z_min)] with increasing D(z), from D(0) = 0 to D(z_max) at the fluorescence maximum, has a mean value of 0.43 (and standard deviation of 0.043) in the Oct/Nov ECNP data, and a mean of 0.57 (and standard deviation of 0.14) in the Jun/Jul ECNP data. No significant correlation was found, within the ECNP province, between variations in B_f and K490 in either of these subsamples. In Table 2, to allow uniform application of equation (8), the appropriate mean B_f has been to A_z with B_z = 0.000 for each time period in the ECNP province.

Variations of B_f with ln[K490 - 0.02] in the AG Jun/Jul (*; dash-dot-dash line) and CCS-Oct (+; solid line) subsamples are illustrated in Figure 11. As was the case with the surface intercepts associated with these subsamples (Fig. 10a), the CCS-October fit (r*r = 0.62, with regression significant at the 0.99 level) is better than that for the AG Jun/Jul subsample (r*r = 0.49, with regression significant at the 0.95 level). Coefficients A_z and B_z to predict B_f with equation (8) in each period are listed in Table 2. The regression models are obviously different for the two provinces and times of year. The CCS-November stations (#), which were not included in either regression, cluster close to the AG Jun/Jul regression line in Fig. 11, but there are too few data points from the CCS province in this month to attach much significance to this proximity.

The use of this model to generate a vertical profile of chlorophyll-a, given remotely sensed K490, is straightforward. The optical depth model [equation (2) with coefficients from Table 1] is first applied to 1/K490 to calculate a vertical profile of optical depth D(z). Coefficients A_c, B_c, A_m, B_m, A_o, B_o, A_z and B_z (appropriate to the biooptical province and time period in question) are taken from Table 2 and substituted in equations (5) through (8) to calculate the profile parameters z_max, D(z_min), ln[Fl(0)/Fl(z_min)], and B_f respectively. These four parameters are subsituted, together with D(z), in equation (3) [for 0 < D(z) < D(z_max)] or (4) [for D(z_max) <

$D(z) < D(z\_min)]$, to calculate $\ln[Fl(z)/Fl(z\_min)]$ at each depth z. At depths where $D(z) > D(z\_min)$, $\ln[Fl(z)/Fl(z\_min)] = 0$.

The performance of the optical attenuation and chlorophyll-a fluorescence profile models are illustrated for five stations each from the Jun/Jul and Oct/Nov subsamples in Figs. 12 and 13 respectively. The profiles illustrated in Fig. 12 are distributed geographically from approximately 28N to 57N near 150W (Fig. 1: circles on cruise track "D") and include examples from ECNP and AG provinces in June-July 1985. The profiles of Fig. 13 are distributed zonally near 34N from 121W (over the inner continental slope) to 140W (Fig. 1: circles on cruise track "A") and characterize the optical variability in transition from the CCS to ECNP central gyre water masses in October 1982. Optical depth profiles calculated with equation (2) and Table 1 coefficients (solid line) are superimposed on the measured profiles of D(z) in Figs. 12a (Jun/Jul: "+") and 13a (Oct/Nov" "o"). Each normalized chlorophyll-a fluorescence profiles $\ln[Fl(z)/Fl(z\_min)]$ is plotted against optical depth D(z) in Figs. 12b (Jun/Jul" "+") and 13b (Oct/Nov: "o"), and superimposed on log-linear equilibrium fluorescence profiles estimated: 1) from a direct least squares fit to the data (dash line), and 2) from optical remote sensing depth 1/K490 (taken from the irradiance profile) using the combined models of the diffuse optical depth [eqn. (2) and Table 1] and log-linear equilibrium fluorescence profiles [eqns. (3) thru (8) and Table 2] (solid

line). The chlorophyll-a fluorescence profiles over depth, obtained by combining the curves of panels a and b of each figure, are superimposed in Figs. 12c (Jun/Jul: "+") and 13c (Oct/Nov: "o") on Fl(z)/Fl(z_min) profiles obtained via the equilibrium profile least squares fit over measured D(z) (dashed curves), and on profiles modeled from K490 (solid curves).

The contrast in ECNP biooptical profile models between Jun/Jul (solid curves) and Oct/Nov (dash curves) is illustrated in Fig. 14 for values of optical remote sensing depth 1/K490 = 25, 30, 35, 40, and 45 m (left to right respectively). Optical depth profile models [eqn. (2) with Table 1] for each 1/K490 for the two time periods are compared in panel 14a. Log-linear equilibrium chlorophyll-a fluorescence profile models [eqns. (3) thru (8) with Table 2] for the two time periods are overlaid in panel 14b. And finally, the resulting vertical profiles of normalized chlorophyll-a fluorescence Fl(z)/Fl(z_min), modeled by combining the associated D(z) and ln{Fl[D(z)]/D(z_min)} profiles from panels 14a and 14b for each 1/K490, are compared in Fig. 14c. This last display (Fig. 14c) clearly reveals that the temporal change in dependencies on 1/K490 of the ECNP diffuse optical depth model [Fig. 5 and Table 2] and equilibrium fluorescence profile model parameters [Figs. 8, 9, 10b, and the shift in B_f; Table 2] combine to manifest a deepening and weakening of the deep chlorophyll-a fluorescence maximum between Jun/Jul (mid-summer) and Oct/Nov (early in the fall transition,

when the top of the nutricline is still at least 40 to 50 m below the top of the seasonal pycnocline).

Biooptical Variability Estimates from CZCS Data.

Fig. 15 is a photographic grey shade display of the provisional summer mean (June-August) K490 distribution calculated as a composite average of CZCS estimates in these months from 1979 through 1985. Light areas correspond to large K490 and dark grey shades to low K490 (or high and low phytoplankton pigment concentrations respectively. The relatively large patches of black centered near 48N, 160W represent the ocean areas which were not observed even once in all 7 years during these months.

The K490 distribution in Fig. 15 provide a biooptical visualization of many well known features of the large scale circulation in the Northeast Pacific Ocean. The ECNP central gyre water masses, characterized by $0.022 < K < 0.05$ m**-1 (45 m > 1/K490 > 20 m) extend from 30N to the SAF near 42N, and from approximately 127W (at the base of the continental slope) to 165W in this map image. The zonal SAF near 42N appears in the map as a wavy biooptical ridge extending from 165W to approximately 135W, where it appears to blend into the more patchy bioptical structure associated with the circulation in the Gulf of Alaska. A preliminary comparison with bathymetry indicates that many of the low transparency (high K490) patches in the Gulf of Alaska are located over or near seamounts (a few of which rise to within

a few hundred m of the surface). The CCS appears as a region of high K490 due to rich biological production associated with coastal upwelling throughout each summer. It is interesting that in even this long term average, CZCS K490 patterns show recognizable vestiges of mesoscale eddies and cross-shelf jets off Pt. Reyes and Pt. Conception, which are often observed in individual satellite images. These phenomena are clearly persistent features of the CCS circulation.

The meridional distribution of optical remote sensing depth 1/K490 extracted from the CZCS Summer Mean K490 (Fig. 15) is profiled along the 150W meridian in Fig. 16, together with the attenuation depths Z_10%, Z_1% and Z_0.1% calculated with the regression model illustrated in Fig. 3. A quantitative comparison is not as encouraging. The CZCS composite mean 1/K490 values (near 150W) are systematically less than those measured aboard the R/V Discoverer in 1985 (Pak et al., 1988; examples illustrated in Fig. 12) by an average factor of 0.67 at ECNP and 0.5 at SAF and AG station latitudes. As a direct consequence of this apparently systematic underestimation of 1/K490, the attenuation depths Z_10%, Z_1%, and Z_0.1% are all also underestimated by proportionate amounts.

In Fig. 17, the CZCS 1/K490 meridional profile at 150W is shown with the derived profiles of the depth (z_max) and strength Fl(z_max)/Fl(z_min) of the normalized chlorophyll-a fluorescence maximum, as calculated with the equilibrium profile model. As a

result of the apparent underestimation of 1/K490 from the CZCS data, the modeled depth of the chlorophyll maximum is significantly shallower than observed aboard Discoverer in 1985 (Pak, et al. 1988), and the magnitude of the fluorescence peak is also underestimated.

DISCUSSION and CONCLUSIONS

The foregoing analyses of in situ biooptical profiles constitute an internally consistent characterization of geographically distinct biooptical provinces (Fig. 1) of the Northeast Pacific Ocean during summer. The ECNP-SAF-AG province transition can be readily distinguished in this season through a combination of climatology and ocean color estimates of K490 (Fig. 15). The ECNP-CCS boundary must, on the other hand, be identified independently from either concurrent or climatological temperature/salinity observations. The results demonstrate that important characteristics of the vertical profiles of both irradiance attenuation (diffuse optical depth) and normalized chlorophyll-a fluorescence can be quantitatively estimated from consistent values of optical remote sensing depth 1/K490; here, "consistent" 1/K490 values were derived directly from the measured irradiance profiles in each case. The overall biooptical characterization of the regions during summer may be summarized through 7 major points of discussion:

1. The vertical profiles of diffuse optical depth D(z) and normalized in situ chlorophyll-a fluorescence Fl(z)/Fl(z_min) may be interrelated by a log-linear equilibrium profile of fluorescence over diffuse optical depth, ln{Fl[D(z)]/Fl(z_min)}, of the form illustrated in Fig. 2c. Examples of the log-linear equilibrium profile

fit to the measured data were illustrated in Figs. 12b and 13b (above). Close inspection of some profiles (e.g. in Fig. 13b) suggests that a small, but systematic, residual curvature may exist. Nevertheless, the log-linear profile fit (Fig. 2c) is a remarkably robust first order approximation, accounting for more than 90% of variance in fluorescence over D(z) in 44 of 52 profiles, and more than 80% in 6 of the remaining 8 [the 2 poorly fit profiles (r*r = 0.7) were measured at a single nearshore station off California in November 1982].

2. The vertical profile of optical depth can be predicted from optical remote sensing depth 1/K490 (m) as a 6 layer model extending from the surface to D(Z_0.1%) = 6.31. A distinct break in the slopes of the regression equations at each depth appears near 1/K490 = 20 m in both Jun/Jul and Oct/Nov data sets; we can offer no explanation of why this optical remote sensing depth is apparently critical and have little choice but to pragmatically report separate equations for the ranges of 1/K490 above and below it. In the range 1/K490>20m, the changes in slope of each Z_n line (and the progressive increase in that change with increasing optical depth) are interpreted as the direct result of a progressive weakening of the deep maximum chlorophyll biomass in oligotrophic ECNP water masses. This trend is attributed intuitively to

progressive nutrient depletion through the course of the summer, during which the seasonal surface mixed layer remains shallow and well isolated from the top of the nitricline.

3. The depth z_max (m) of the chlorophyll-a fluorescence maximum is predicted from optical remote sensing depth 1/K490 (m) with separate regression coefficients for Jun/Jul (ECNP, SAF and AG) and Oct/Nov (ECNP and CCS-Oct) (Fig. 8). At both times of year, an increase in z_max is clearly associated with an increase in 1/K490 (implying a decrease in near surface pigment biomass). The offset between the two regression lines indicates that with increasing time, during the period of summer mixed layer stratification, the z_max associated with a given 1/K490 becomes progressively deeper in all provinces.

4. The optical depth of the deep background fluorescence minimum D(z_min) is predicted as a logarithmic function of remote sensing [K490 - 0.02], which is directly related (in the formalism of ocean color algorithms) to remote sensing pigment biomass. D(z_min) may be interpreted as the total vertical span (in optical depth) over which light adaptation by marine phytoplankton determines the coupled equilibrium profiles of D(z) and ln(Fl[D(z)]/Fl(z_min)). The slopes of the regression

lines (Fig. 9) indicate that in Jun/Jul D(z_min) systematically decreases with increasing remote sensing K490 (pigment biomass), but that in Oct/Nov it systematically increases with increasing K490. The intersection of the two regression lines corresponds approximately to 1/K490 = 35m. All but one of the stations in ECNP either cluster near the intersection or fall to its left, while all of the Jun/Jul AG and SAF, and the Oct/Nov CCS stations, fall to its right. At face value, the two lines suggest that the regional summer evolution of the optical thickness of the equilibrium chlorophyll-a fluorescence profile may be represented by a rotation of the regression model about the intersection. The basis for this interpretation is weak, however, due especially to the geographically distinct biooptical provinces represented within the Jun/Jul and Oct/Nov subsamples.

5. The slope B_f of the upper segment of the log-linear equilibrium fluorescence profile can be predicted in the AG:Jun/Jul and CCS:Oct using separate regression equations (with considerably more residual scatter in the correlation for the AG subsample). In both provinces, B_f decreases with increasing [K490 - 0.02] (or pigment biomass). The intercepts and slopes of the two regression lines indicate that normalized fluorescence

increases more slowly over optical depth in the AG:Jun/Jul than in the CCS:Oct province, and that the trend becomes more pronounced with increasing [K490 - 0.02] (or pigment biomass).

In the ECNP, the average value of B_f changes significantly between Jun/Jul and Oct/Nov, but variance is small with no apparent dependence on 1/K490 in either time period.

6. The surface intercept of the log-linear equilibrium fluorescence profile ln[Fl(0)/Fl(z_min)] is predicted as a function of remote sensing [K490 - 0.02]. Four statistically different sets of regression coefficients were determined for ECNP:Jun/Jul, ECNP:Oct/Nov, AG:Jun/Jul and CCS:Oct, respectively (Fig. 10).

   The AG:Jun/Jul and CCS:Oct relationships are similar in slope, with the CCS:Oct values biased to lower values (and showing a much tighter fit). In both cases the surface intercept ln[Fl(0)/Fl(z_min)] increases with increasing [K490 - 0.02], and therefore with increasing remote sensing pigment biomass.

   In ECNP during both time periods, the "fit of choice" (refer to the discussion of Fig. 10b in the previous section) gives parallel slopes which indicate a decrease in the surface intercept of the equilibrium profile with

increasing remote sensing [K490 - 0.02] (pigment biomass). This seeming paradox can lead to a great deal of confusion, unless it is borne firmly in mind that the "fluorescence surface intercept" referenced here is not equatable in any direct sense to chlorophyll-a fluorescence measured at the surface alone. Quite aside from its normalization to the deep background fluorescence, the surface intercept is a characteristic parameter of a least squares fit to the log-linear equilibrium fluorescence profile from the surface to D(z_max). Recall that in ECNP in each time period, z_max increases with decreasing K490 and B_f is essentially constant (items 3 and 5 above). Therefore, the change of the surface intercept ln[Fl(0)/Fl(z_min)] with increasing K490 arises from the interaction of the tendencies for z_max and Fl(z_max)/Fl(z_min) to both increase with decreasing K490 (Fig. 14c). The observed negative slopes of the surface intercept regressions implies that ln[Fl(z_max)/Fl(z_min)] increases more slowly than does D(z_max) with decreasing K490.

7. It is plausible to interpret these results from the ECNP province as a temporal evolution in biooptical characteristics through the period extending from mid-summer into the fall transition in Oct/Nov. Assuming the data from two different years can be compared in this

way, the overall effect of the apparent temporal tendencies of regression models applicable to the ECNP province (discussion points 2 through 6 above) represents a progressive weakening and deepening of the deep normalized chlorophyll-a fluorescence maximum associated with a fixed value of 1/K490 (Fig. 14c). This tendency is consistent with a progressive depletion of nutrients in the euphotic zone during summer. The shallow pynocline sustained throughout the period deprives the euphotic water column of turbulent energy, which could otherwise entrain deeper water to replace nutrients exported downward with settling organic particles.

The provisional CZCS-derived estimates of 1/K490, and resulting 3-dimensional estimates of equilibrium profiles of optical depth and normalized chlorophyll-a fluorescence agree qualitatively with the geographic patterns of the in situ measurements. However, the June-August composite mean CZCS 1/K490 values extracted from Fig. 15 along 150W consistently underestimate 1/K490 as measured aboard the R/V Discoverer in Jun/Jul 1985 by mean factors of 0.67 in the ECNP and 0.5 in the SAF and AG (Figs. 13, 15 and 16, and comparison with the other Discovery stations not shown). Fig. 15 is an extremely preliminary product, prepared on an interim basis to facilitate the initial stages of the present research. Part of this discrepancy may represent a departure of the July 1985 biooptical conditions from the

composite average over seven years and three months, but a large fraction of the discrepancy is more likely to to be traced to the preliminary nature of the CZCS sensitivity characterization within the algorithms used to prepare Fig. 15. The internal consistency of the single scattering atmospheric correction algorithm (Gordon, et al., 1983) and sensitivity degradation estimates (Mueller, 1985) were based on previous evaluations of late summer to early fall CZCS data extending only through 1982. Work is now in progress to evaluate the overall CZCS sensor/algorithm system performance, in comparison with in situ biooptical observations (the present results being a first installment), over the entire seven year period, within the framework of the multiple scattering atmospheric correction published by Gordon, Brown and Evans (1988).

The present biooptical province characterization of the Northeast Pacific is clearly both tentative and limited in its spatial and temporal scope. The apparent temporal change in ECNP biooptical profile characteristics, while plausible and temptingly subject to simple interpretation, is best regarded as a working hypothesis to be tested with future observations distributed more evenly over the summer months. In the summer CCS and AG, a wider distribution of sampling over time will be required to detect and quantify symptoms of temporal evolution in the equilibrium biooptical profiles of these important provinces. The four profiles from two closely spaced stations in the CCS during mid-

November 1982 strongly suggest that a major change occurred in the biooptical profile characteristics of the CCS between mid-October and mid-November; however, the sampling is far too anecdotal to confidently conclude that the apparent change was real, let alone to quantitatively characterize it. The few observations from the SAF were sufficient to identify its nature as a separate province, and to qualitatively identify its characteristic optical depth profile as a relatively thin turbid layer overlying a very clear water column, but more data are needed to develop and verify a reliable prediction model. And finally, a comparative description of winter conditions is totally lacking at the present stage of analysis.

The present analyses are a first step in the evolutionary development of an internally consistent climatology of biooptical variability in the Northeast Pacific Ocean. The equilibrium profile model of normalized chlorophyll-a fluorescence over optical depth offers both a robust tool for combined first order characterization of irradiance and fluorescence profiles, and a conceptual framework linking remotely sensed ocean color, through 1/K490, to the vertical profiles of chlorophyll-a fluorescence and optical depth. The present results make it obvious that empirical models relating ocean color to vertical biooptical profiles must use temporally and geographically varying coefficients, but classifications within a reasonable number of biooptical provinces and seasonal periods appears to be within

reach. Many of the deficiencies listed in the previous paragraph will be alleviated through assimilation of additional existing data sets into the biooptical province analysis, together with careful reconciliation of the CZCS K490 and in situ biooptical profiles, as a direct continuation of the present work. And over the next few years, entirely new biooptical data sets will emerge from today's oceanographic field programs. Within the near future, a web of models similar to those presented here can be expected to provide an increasingly complete empirical description of biooptical relationships linking phytoplankton pigment biomass to ocean optical properties and remotely sensed ocean color within and between biooptical provinces in many regions of the world oceans.

ACKNOWLEDGEMENTS

We owe thanks to our colleagues at SDSU CHORS, San Diego, CA: Chuck Trees, for many helpful discussions of the work and recommendations which improved the manuscript, and Ruth Wittenberg-Fay, who assisted with the preparation of volumnous working graphics, as well as the final figures. We are indebted also to Ray Smith (Dept. of Geography, UCSB, Santa Barbara, CA) and Karen Baker (IMR, SIO, UCSD, La Jolla, CA) for allowing our use here of a subset of the BOPS irradiance and fluorescence profiles from our Acania ODEX expedition in 1982, to Hasong Pak and Ron Zaneveld (School of Oceanography, OSU, Corvallis, OR) for use of the irradiance and fluorescence profiles from their R/V Discovery cruise of 1985, and to Ros Austin and Jeff Nolten (IMR, SIO, UCSD, La Jolla, CA) for assistance with analysis of the data acquired by the Visibility Laboratory during the two DeSteiguer cruises in 1982 and 1985. This research was supported by the Oceanographer of the Navy under NORDA contract N00014-87-C-6002 (at the SIO Visibility Laboratory, UCSD, La Jolla, CA) and continues under NORDA contract N00014-89-C-6007 (at SDSU CHORS, San Diego, CA). Portions of the in situ profile analysis were supported under NOSC contract N6601-86-D-0022 (SIO UCSD).

REFERENCES

AUSTIN, R.W. and T.J. PETZOLD. 1981. The determination of the diffuse attenuation coefficient of sea water using the Coastal Zone Color Scanner. In: GOWER, J.F.R. [Ed.], OCEANOGRAPHY FROM SPACE, Plenum. pp239-256.

GORDON, H.R. and D.K. CLARK. 1981. Clear water radiances for atmospheric correction of Coastal Zone Color Scanner imagery. Applied Optics, 20: 4175-4180.

GORDON, H.R., et al. 1983. Phytoplankton pigment concentrations in the Middle Atlantic Bight: comparison of ship determinations and CZCS estimates. Applied Optics, 22: 20-36.

GORDON, H.R., J.W. BROWN and R.H. EVANS. 1988. Exact Rayleigh scattering calculations for use with the Nimbus-7 Coastal Zone Color Scanner. Applied Optics, 27: 862-871.

HAURY, L.R., et al. 1986. Biological consequences of a recurrent eddy off Point Conception, California. J. Geophys. Res., 91: 12937-12956.

HAYWARD, T.L. and E.L. VENRICK. 1982. Relation between surface chlorophyll, integrated chlorophyll and integrated primary production. Mar. Biol., 69: 247-252.

HOVIS, W.A., et al. 1980. Nimbus-7 Coastal Zone Color Scanner: System description and initial imagery. Science, 210:60-63.

MUELLER, J.L. 1985. Nimbus-7 CZCS: confirmation of its radiometric sensitivity decay rate through 1982. Applied Optics, 24: 1043-1047.

MUELLER, J.L. 1988. Nimbus-7 CZCS: electronic overshoot due to cloud reflectance. Applied Optics, 27: 438-440.

NIILER, P.P. and R.W. REYNOLDS. 1984. The three-dimensional circulation near the Eastern North Pacific subtropical front. J. Phys. Oc., 14:217-230.

PAK, H., D.A. KIEFER, and J.C. KITCHEN. 1988. Meridional variations in the concentration of chlorophyll and microparticles in the North Pacific Ocean. Deep-Sea Res., 35:1151-1171.

PLATT, T. and S. SATHYENDRANATH. 1988. Oceanic primary production: Estimation by remote sensing at local and regional scales. Science, 241: 1613-1620.

RODEN, G.I. 1975. On North Pacific temperature, salinity, sound velocity and density fronts and their relation to the wind and energy flux fields. J. Phys. Oc., 5: 557-571.

RODEN, G.I. 1977. Oceanic subarctic fronts of the central Pacific; stucture of and response to atmospheric forcing. J. Phys. Oc., 7:761-778.

TABLE 1

IRRADIANCE ATTENUATION PROFILE MODEL COEFFICIENTS

June/July (1985)

1/K490 < 20 m

n(%)	D(Z_n)	A_n (m)	B_n	r*r	S_xy (m)
10.0	2.30	1.26(1.50)	2.193(0.072)	0.95	1.67
3.0	3.51	3.34(2.73)	3.144(0.131)	0.93	3.03
1.0	4.61	4.79(4.79)	4.373(0.230)	0.89	5.32
0.3	5.81	17.05(7.09)	5.243(0.341)	0.84	7.89
0.1	6.91	21.16(8.96)	6.668(0.417)	0.82	9.36

June/July (1985)

1/K490 > 20 m

n(%)	D(Z_n)	A_n (m)	B_n	r*r	S_xy (m)
10.0	2.30	-0.10(4.34)	1.763(0.084)	0.94	4.56
3.0	3.51	10.11(6.24)	2.060(0.121)	0.90	6.56
1.0	4.61	34.59(6.21)	2.002(0.120)	0.90	6.53
0.3	5.81	70.79(6.85)	1.848(0.132)	0.86	7.21
0.1	6.91	92.69(7.74)	2.060(0.146)	0.87	7.60

October/November (1982)

1/K490 < 20 m

n(%)	D(Z_n)	A_n (m)	B_n	r*r	S_xy (m)
10.0	2.30	1.69(1.49)	2.251(0.078)	0.97	1.46
3.0	3.51	10.17(3.32)	2.781(0.174)	0.90	3.27
1.0	4.61	23.08(3.90)	2.934(0.205)	0.87	3.84
0.3	5.81	33.00(3.77)	3.682(0.198)	0.92	3.70
0.1	6.91	46.70(5.72)	4.383(0.312)	0.88	5.19

October/November (1982)

1/K490 > 20 m

n(%)	D(Z_n)	A_n (m)	B_n	r*r	S_xy (m)
10.0	2.30	12.96(1.76)	1.669(0.039)	0.87	3.70
3.0	3.51	19.60(3.14)	2.232(0.069)	0.79	6.60
1.0	4.61	28.45(4.51)	2.672(0.099)	0.78	8.75
0.3	5.81	25.71(5.91)	3.680(0.124)	0.79	10.38
0.1	6.91	49.96(7.40)	3.903(0.161)	0.78	10.88

Table 2

CHLOROPHYLL-A FLUORESCENCE PROFILE MODEL COEFFICIENTS

Depth of Fluorescence Maximum
ln[z_max], Equation (5)

Province/Month:	A_c [ln(m)]	B_c	r*r	S_xy [ln(m)]
A,E,G	0.367(0.091)	1.094(0.020)	0.95	0.134
B,C,F	1.017(0.073)	0.986(0.015)	0.91	0.136

Optical Depth of Minimum Fluorescence
ln[D(z_min)], Equation (6)

Province/Month:	A_m	B_m	r*r	S_xy
A,F,G	1.666	-0.0463	0.38	0.084
B,C,D,F	2.433	0.1140	0.71	0.069

Surface Chlorophyll-a Fluorescence
ln[Fl(0) / Fl(z_min], Equation (7)

Province/Month:	A_o	B_o	r*r	S_xy
G, E(?), F(?), D(?)	3.856	0.6920	0.50	0.394
C, D(?), E(?)	3.577	0.9883	0.93	0.208
A	-0.681	-0.1246	0.62	0.071
B	-0.775	-0.1150	0.44	0.050

Slope of Fluorescence over D(z) (z < z_max)
B_f, Equation (8)

Province/Month:	A_z	B_z	r*r	S_xy
G, E(?), F(?), D(?)	-1.201	-0.4689	0.490	0.274
C, F(?)	0.107	-0.1953	0.618	0.121
A	0.570	0.0000	---	0.143
B	0.430	0.0000	---	0.043

BIOOPTICAL PROVINCE/MONTH(s) KEY:

A: ECNP / June-July 1985
B: ECNP / October-November 1982
C: CCS / October 1982
D: CCS / November 1982
E: SAF / July 1985
F: SAF / November 1982
G: Gulf of Alaska / July 1985

FIGURE CAPTIONS

Figure 1: Biooptical Provinces of the Northeast Pacific. The dashed lines represent provisional geographic boundaries of four biooptically distinct provinces associated with well known features of the regional ocean circulation: the California Current System (CCS), the Alaskan Gyre (AG), the N. Pacific Subarctic Front (SAF), and the oligotrophic water masses of the East Central North Pacific central gyre (ECNP). The dotted line along 33N marks the approximate location of the Subtropical Front (STF). Irradiance profiles used for the classification were acquired at stations along cruise tracks (solid lines) aboard the R/V Acania in Oct/Nov 1982 ("A"), the USNS DeSteiguer in Oct/Nov 1982 ("B"), the USNS DeSteiguer in June 1985 ("C"), and the R/V Discoverer in Jun/Jul 1985 ("D"); fluorescence profiles were measured on tracklines A and D. Circles on tracks A and D mark locations of example profiles in Figs. 12 and 13, respectively.

Figure 2: Conceptual model relating vertical profiles of normalized chlorophyll-a fluorescence Fl(z)/Fl(z_min) and optical depth D(z) to optical remote sensing depth 1/K490 (m). Depths (m) z_max of the chorophyll-a fluorescence maximum, z_min of the deep background

fluorescence minimum, and 1/K490 are marked on the curves of panels a and b, and the corresponding optical depths D(z_max), D(z_min) and D(1/K490) are marked on the log-linear equilibrium profile of panel c.

Figure 3: Regression model predicting the vertical profile of irradiance attenuation from optical remote sensing depth 1/K490 in ECNP (o) and AG (*) in Jun/Jul (1985). The regression lines (dashed) relate 1/K490 (m) to the depths Z_n where E(Z_n) is attenuated to 10%, 3%, 1%, 0.3% and 0.1% of E(0) (from bottom to top, respectively). Separate families of regression lines are given for 1/K490 < 20m and 1/K490 > 20m [equation (2) and Table 1]. Scatter is shown for measured attenuation depths Z_10%, Z_1% and Z_0.1% only.

Figure 4: Same as Fig. 3 for ECNP (o) and CCS (+) near 34N in Oct/Nov (1982).

Figure 5: Regression models of Z_n on 1/K490 for Jun/Jul (dash lines from Fig. 3) and Oct/Nov (dash--dash lines from Fig. 4) compared.

Figure 6: Depths Z_n (m) of 10%, 1% and 0.1% light levels from irradiance profiles in the Bering Sea (June 1985 "b"), compared with regression lines from Fig. 3.

Figure 7: Depths Z_n (m) of 10%, 1% and 0.1% light levels from irradiance profiles in SAF near 42 N, 150 W (Nov 1982 "X" and Jun 1985 "x") compared with regression lines from Fig. 3.

Figure 8: Logarithmic regression models predicting z_max (depth of maximum chlorophyll-a fluorescence) from 1/K490 (optical remote sensing depth) for ECNP and AG in Jun/Jul (dash line) and ECNP and CCS in Oct/Nov (dash - - dash line). Refer to Table 2 and equation (5) in the text. Scatter of the Jun/Jul observations from ECNP (o), SAF (x) and AG (*) stations is illustrated in panel 8a. Scatter of Oct/Nov observations from ECNP (o), CCS-Oct (+) and CCS-Nov (#; excluded from the regression fit) is illustrated in panel 8b.

Figure 9: Logarithmic regression models predicting D(z_min) (optical depth of the deep background fluorescence minimum) from remotely sensed [K490-0.02], where 0.02 is the approximate value of K(490) for pure water, for ECNP and AG in Jun/Jul (dash line) and for ECNP and CCS in Oct/Nov (dash--dash line) [eqn. (6); Table 2]. Scatter of Jun/Jul measurements at ECNP (o), SAF (x) and AG (*) stations is illustrated in panel 9a. Scatter of Oct/Nov data from ECNP (o), CCS-Oct (+) and CCS-Nov (#) is shown in panel 9b.

FIGURE 2

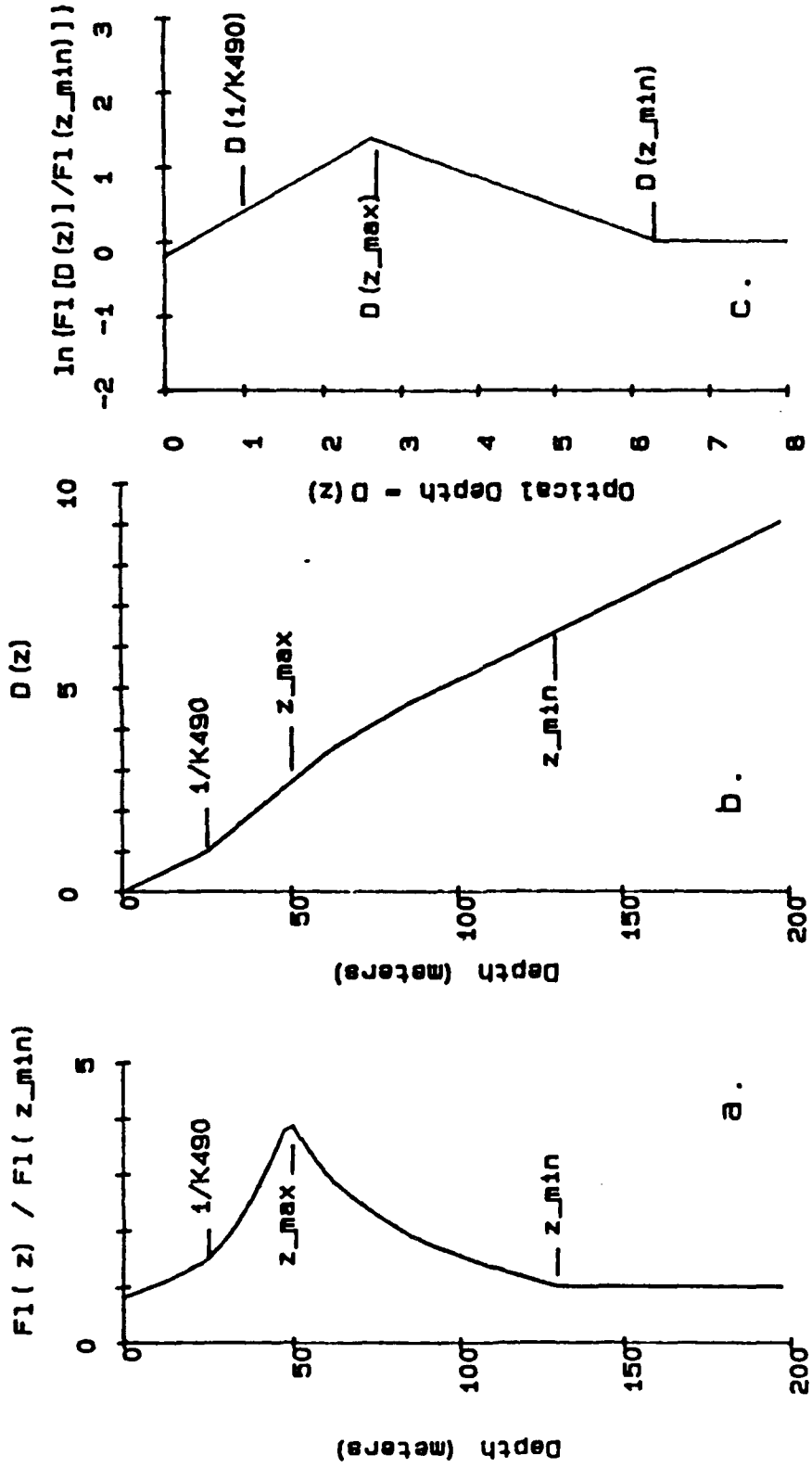
ln(F1[D(z)]/F1(z_min))
D(1/K490)
D(z_max)
D(z_min)
c.
Optical Depth = D(z)
D(z)
1/K490
z_max
z_min
b.
Depth (meters)
F1(z) / F1(z_min)
1/K490
z_max
z_min
a.
Depth (meters)

FIGURE 3

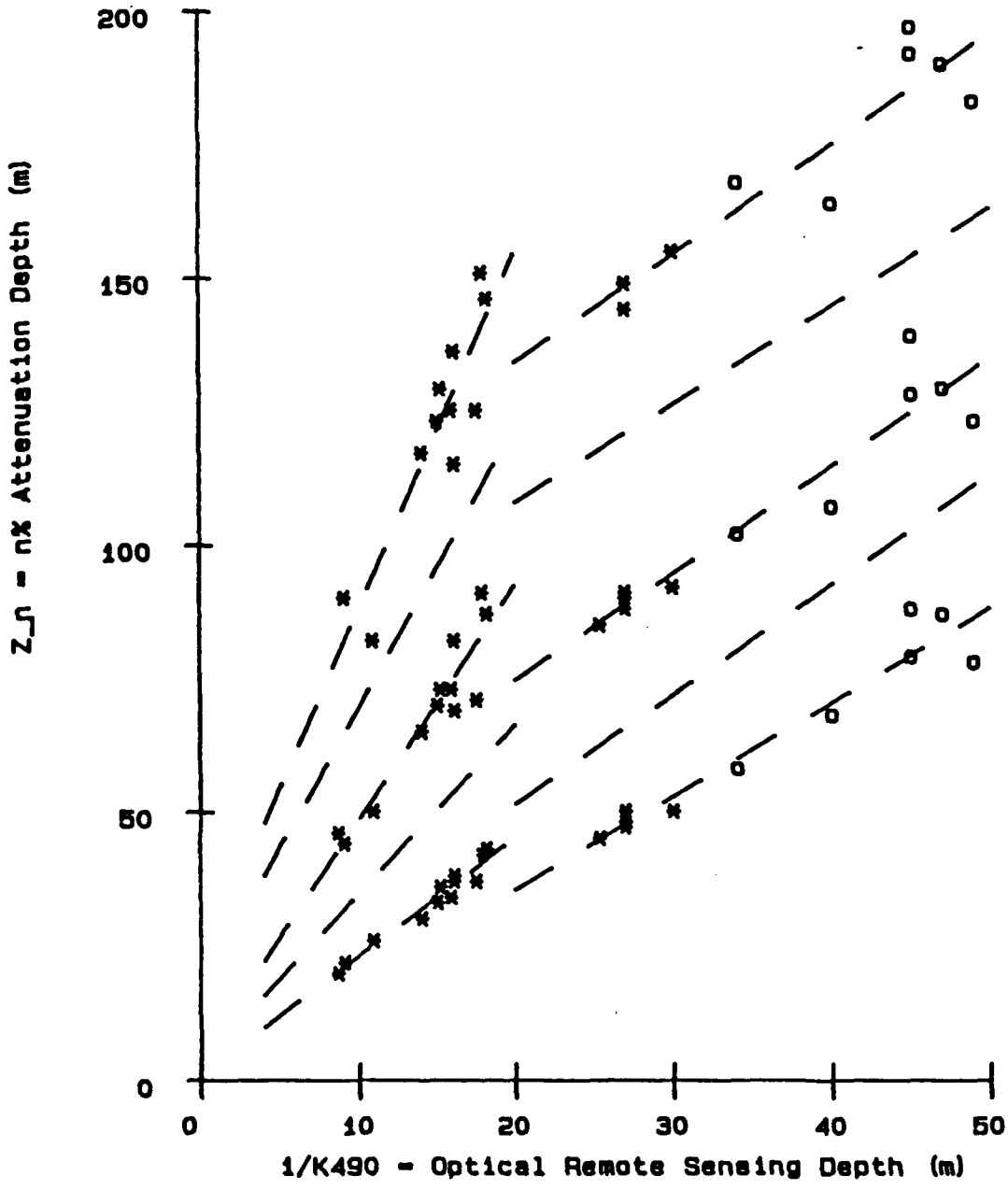
200
150
100
50
0
Z_n = n% Attenuation Depth (m)
0
10
20
30
40
50
1/K490 = Optical Remote Sensing Depth (m)

FIGURE 4

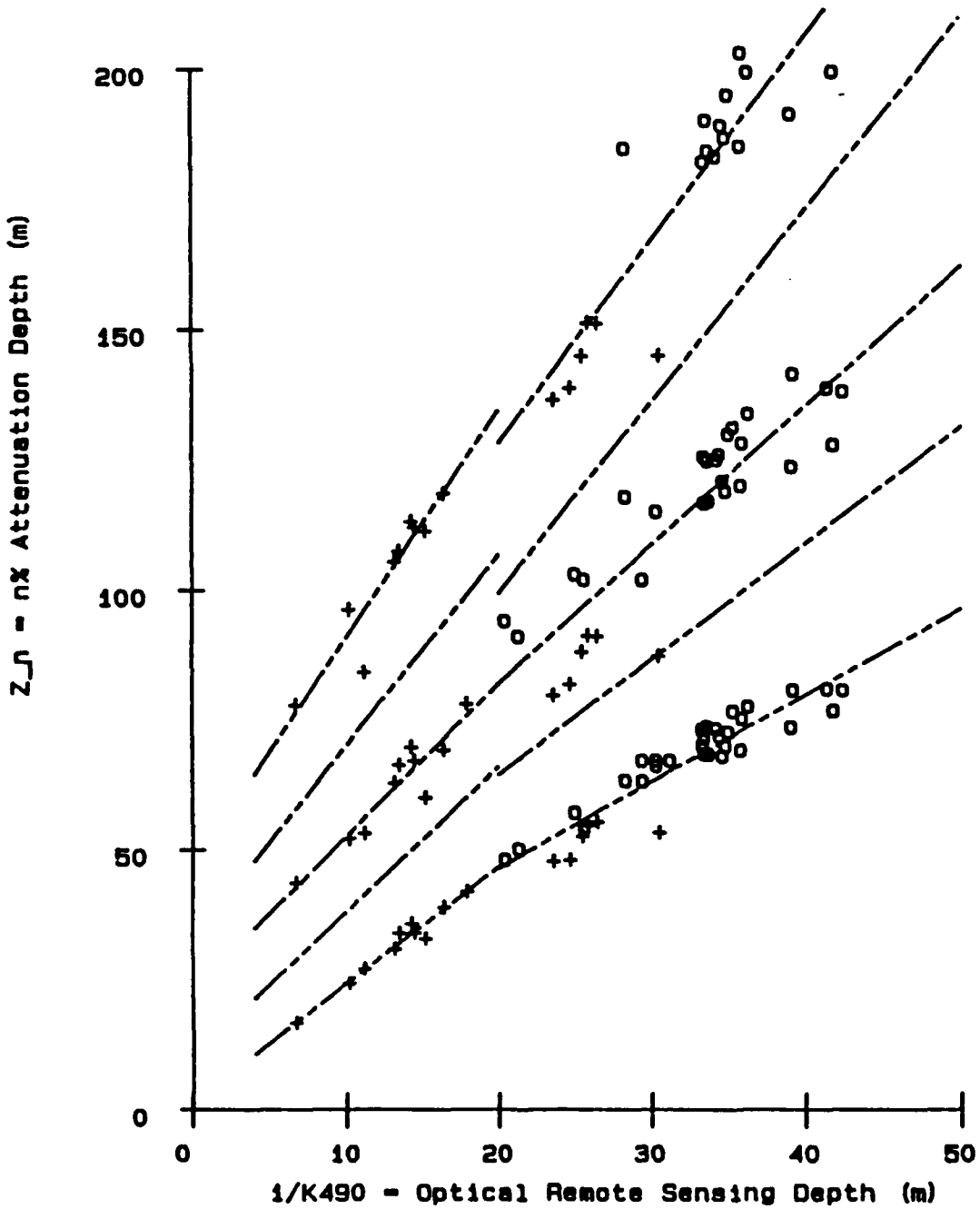
200
150
100
50
0
0
10
20
30
40
50
Z_n = n% Attenuation Depth (m)
1/K490 = Optical Remote Sensing Depth (m)

FIGURE 5

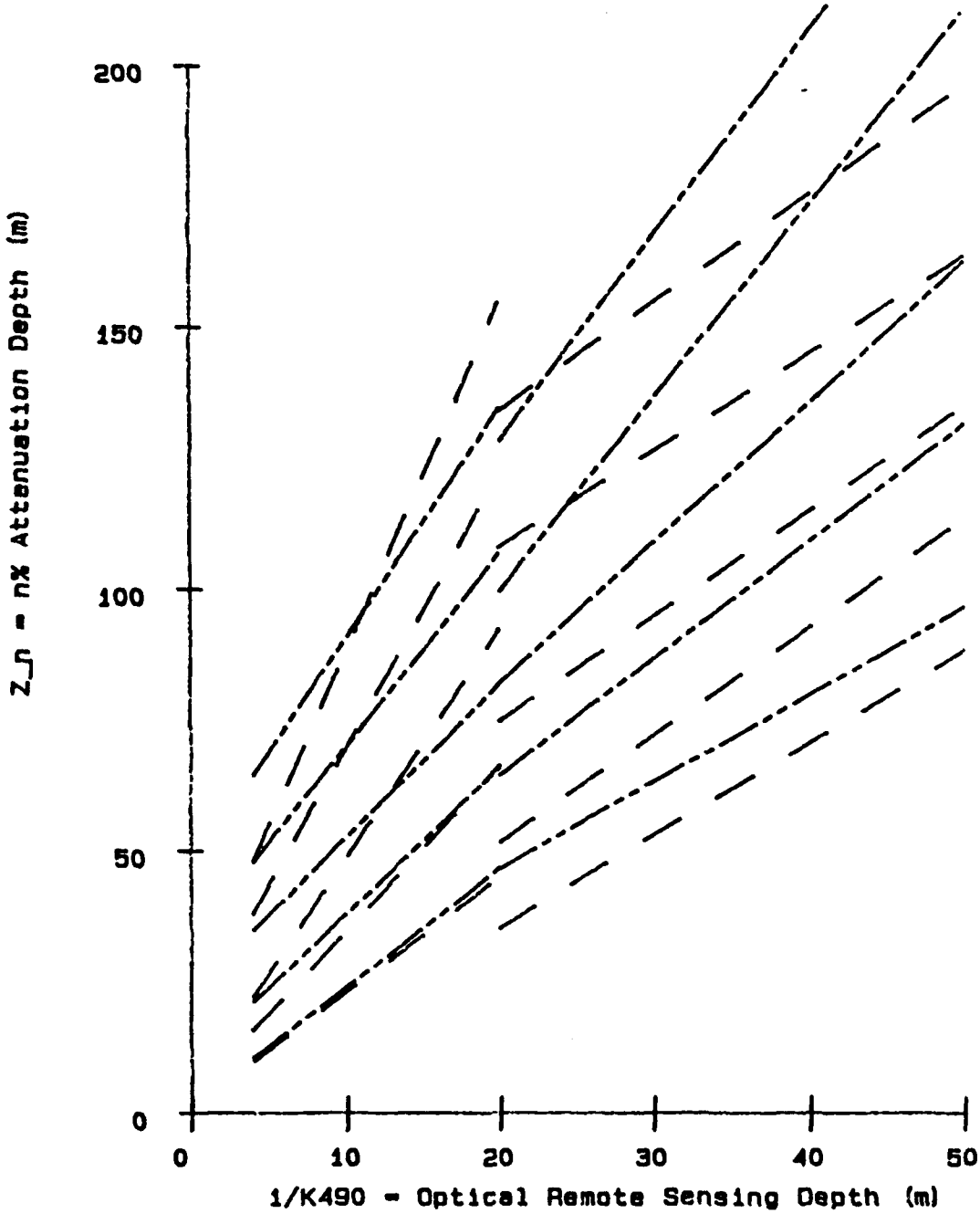
200
150
100
50
0
Z_n = n% Attenuation Depth (m)
0
10
20
30
40
50
1/K490 = Optical Remote Sensing Depth (m)

FIGURE 6

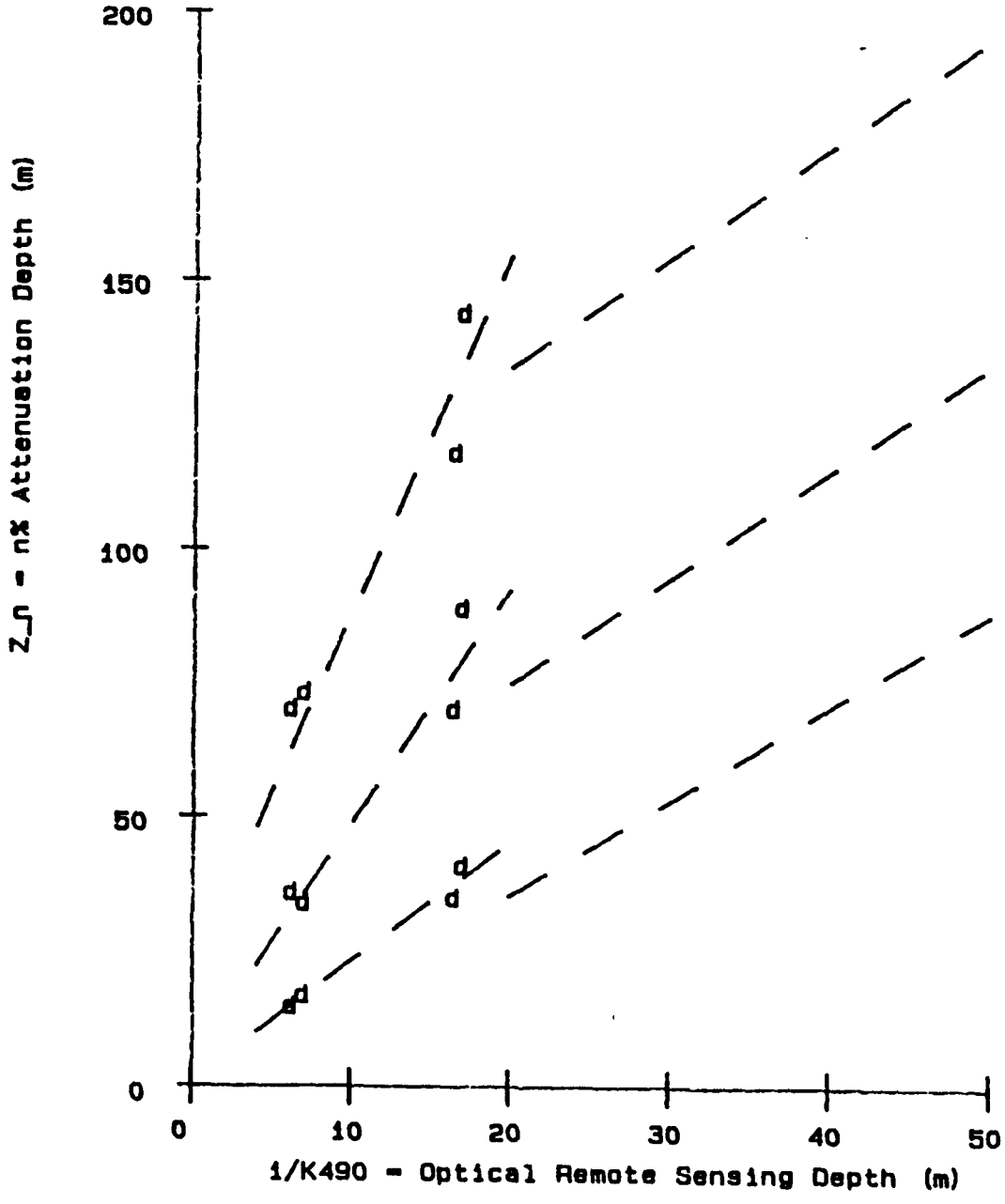
200
150
100
50
0
Z_n = n% Attenuation Depth (m)
0
10
20
30
40
50
1/K490 = Optical Remote Sensing Depth (m)

FIGURE 7

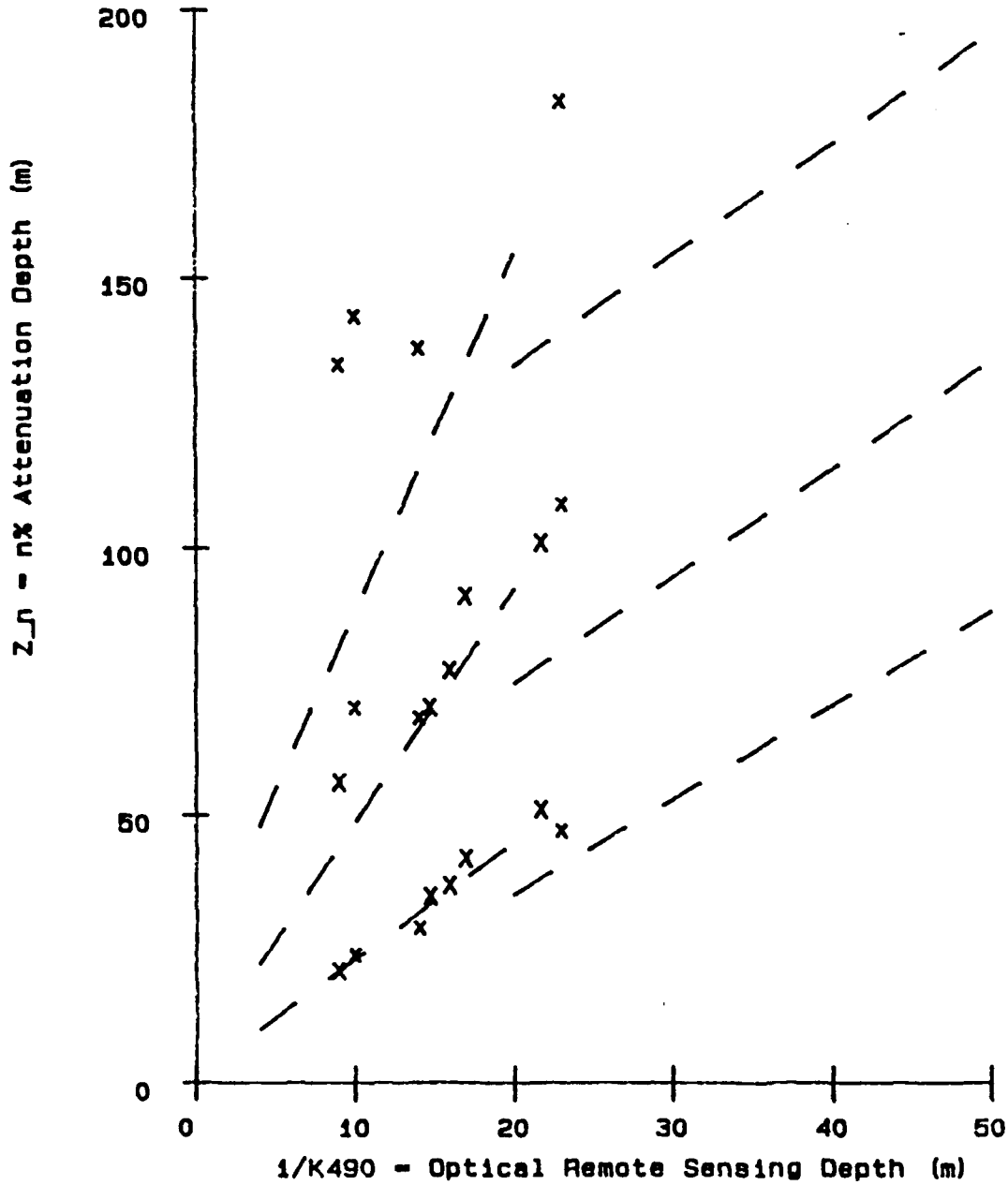
200
150
100
50
0
Z_n = n% Attenuation Depth (m)
0
10
20
30
40
50
1/K490 = Optical Remote Sensing Depth (m)

FIGURE 8a

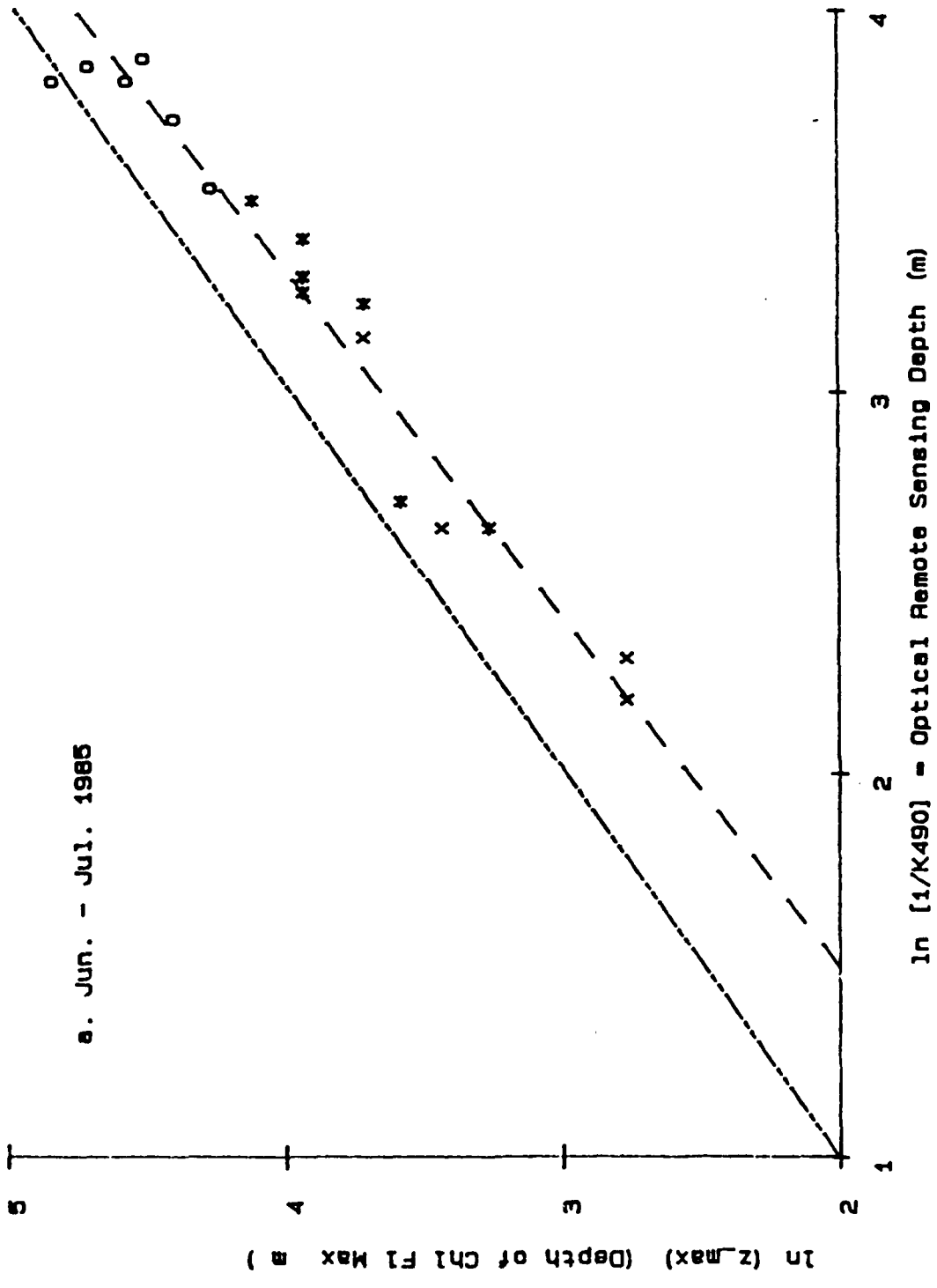
a. Jun. - Jul. 1985
ln (z_max) (Depth of Chl F1 Max m)
ln [1/K490] = Optical Remote Sensing Depth (m)
1
2
3
4
5

FIGURE 8b

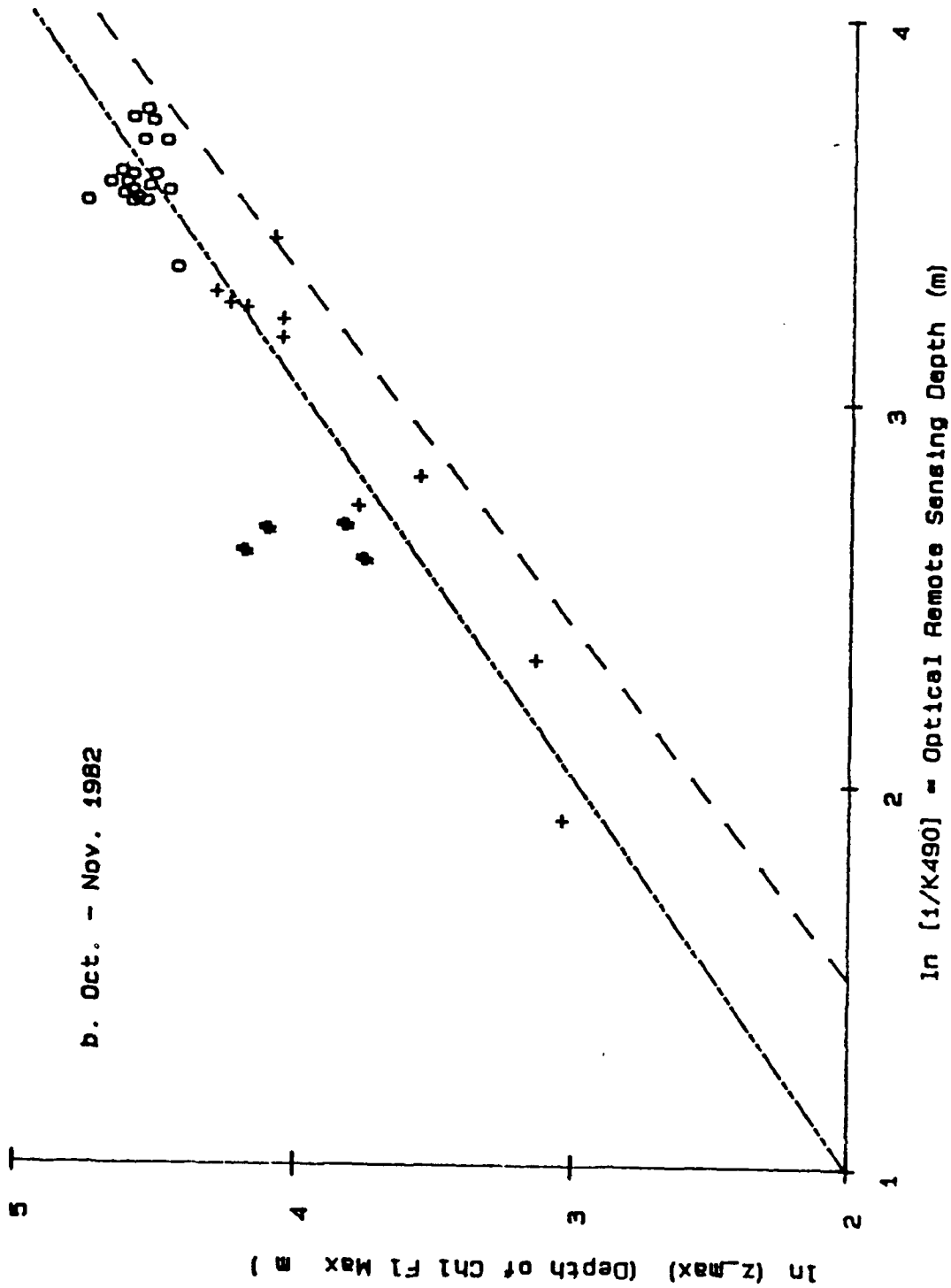
b. Oct. - Nov. 1982
ln (z_max) (Depth of Chl F1 Max m)
ln (1/K490) = Optical Remote Sensing Depth (m)
1
2
3
4
5

FIGURE 9a

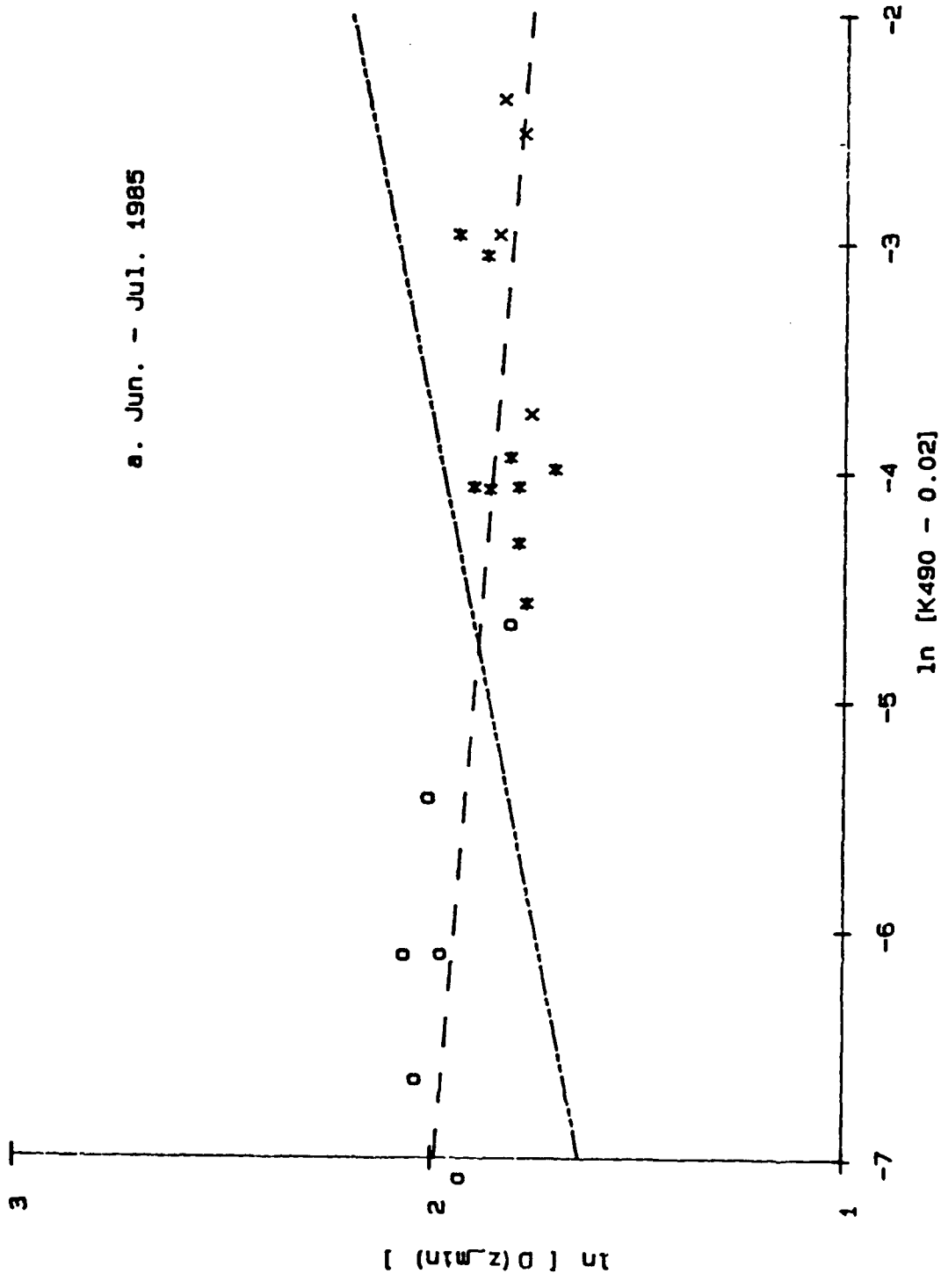

FIGURE 9b

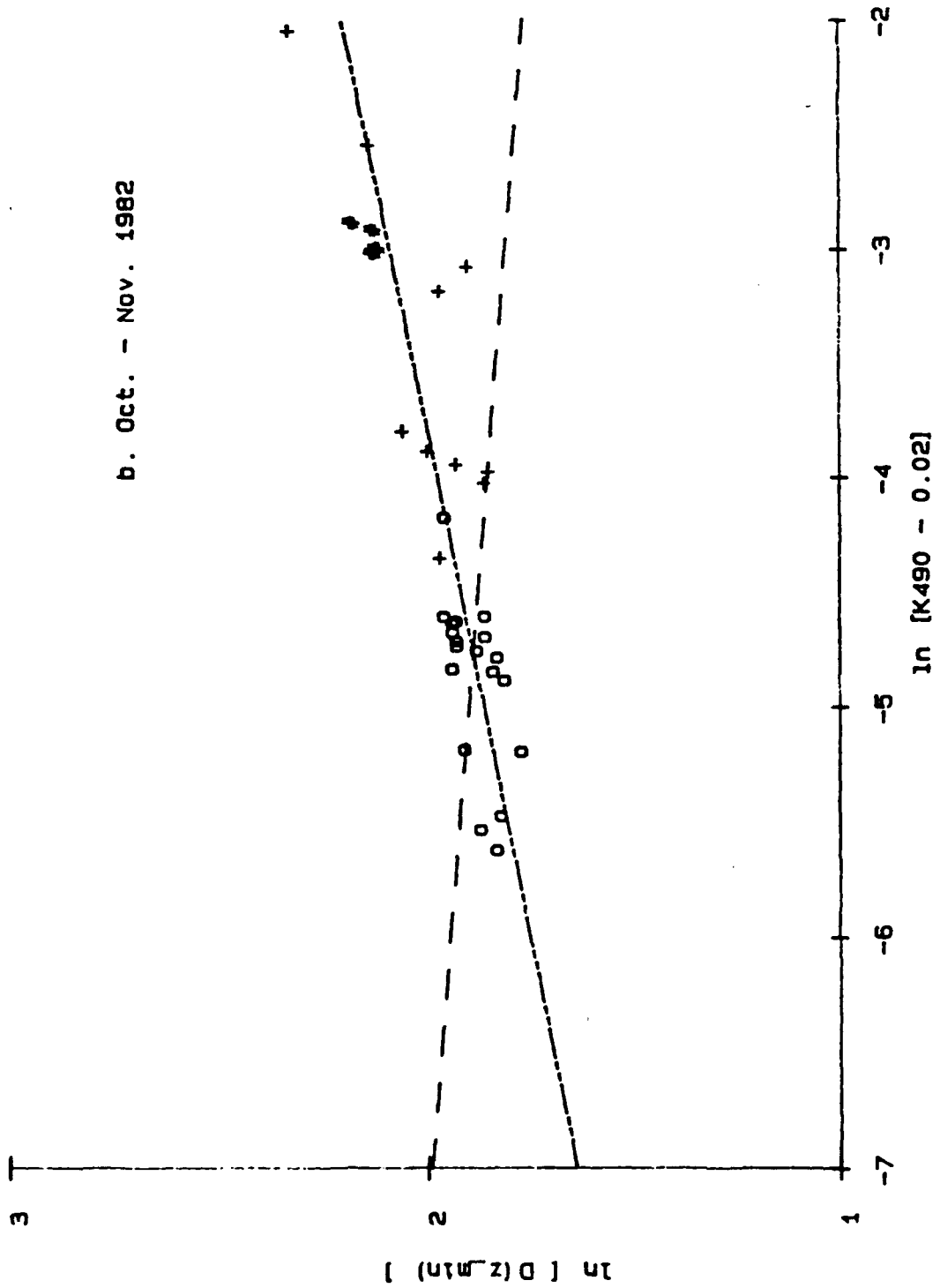

FIGURE 10a

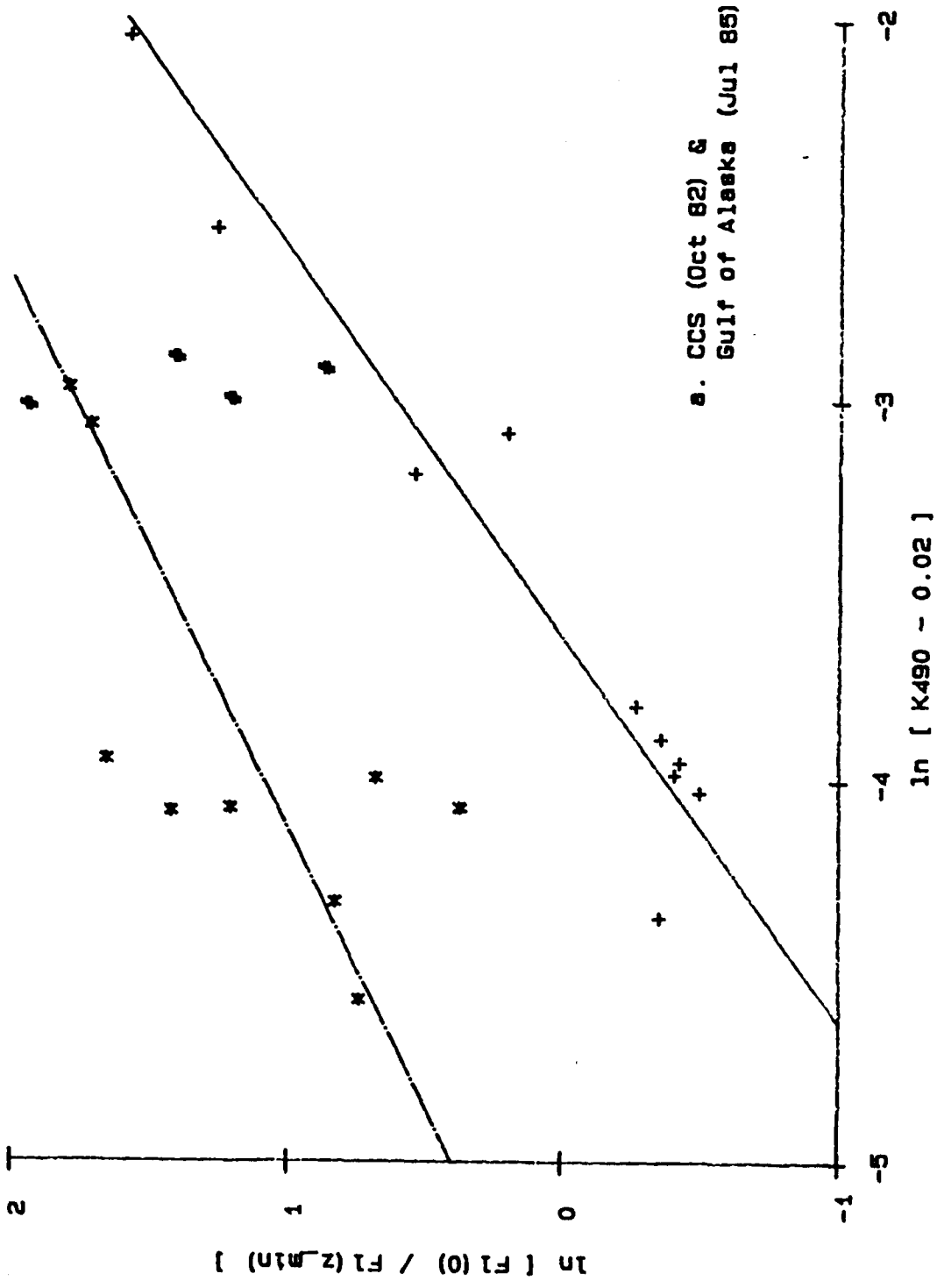
a. CCS (Oct 82) &
Gulf of Alaska (Jul 85)
ln [K490 - 0.02]
-2
-3
-4
-5
ln [F1 (0) / F1 (z_min)]
2
1
0
-1

FIGURE 10b

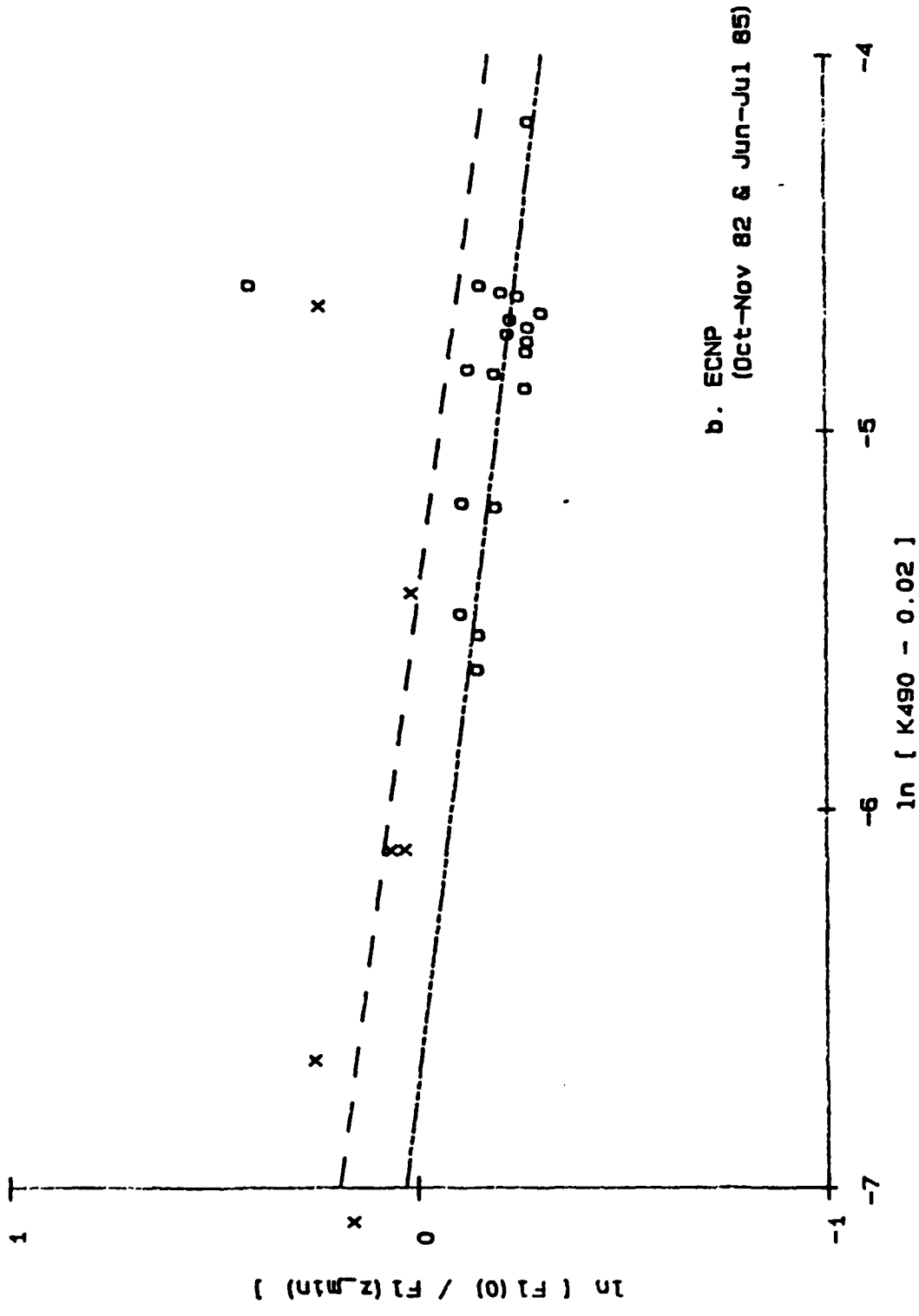

FIGURE 11

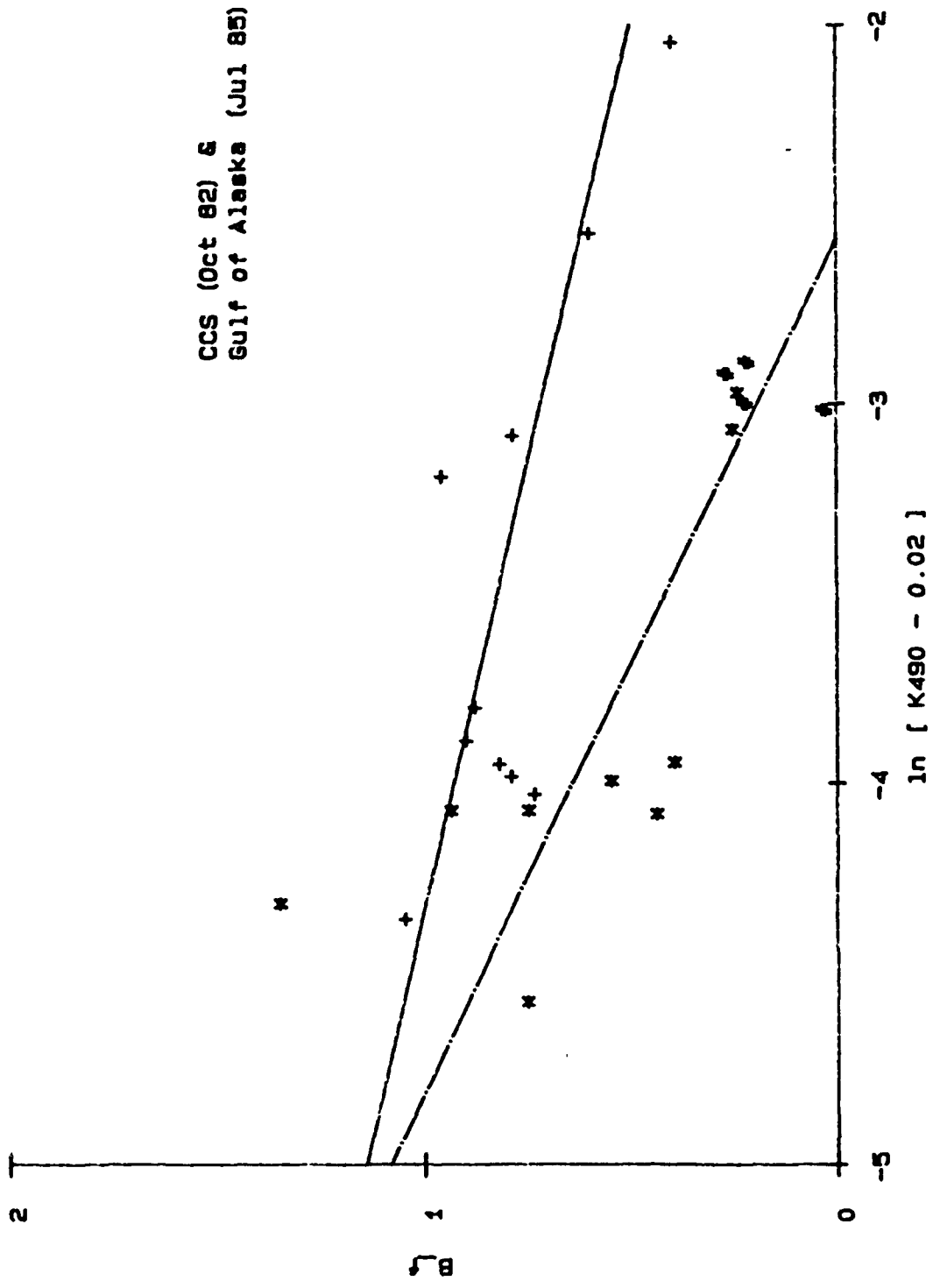

FIGURE 12a

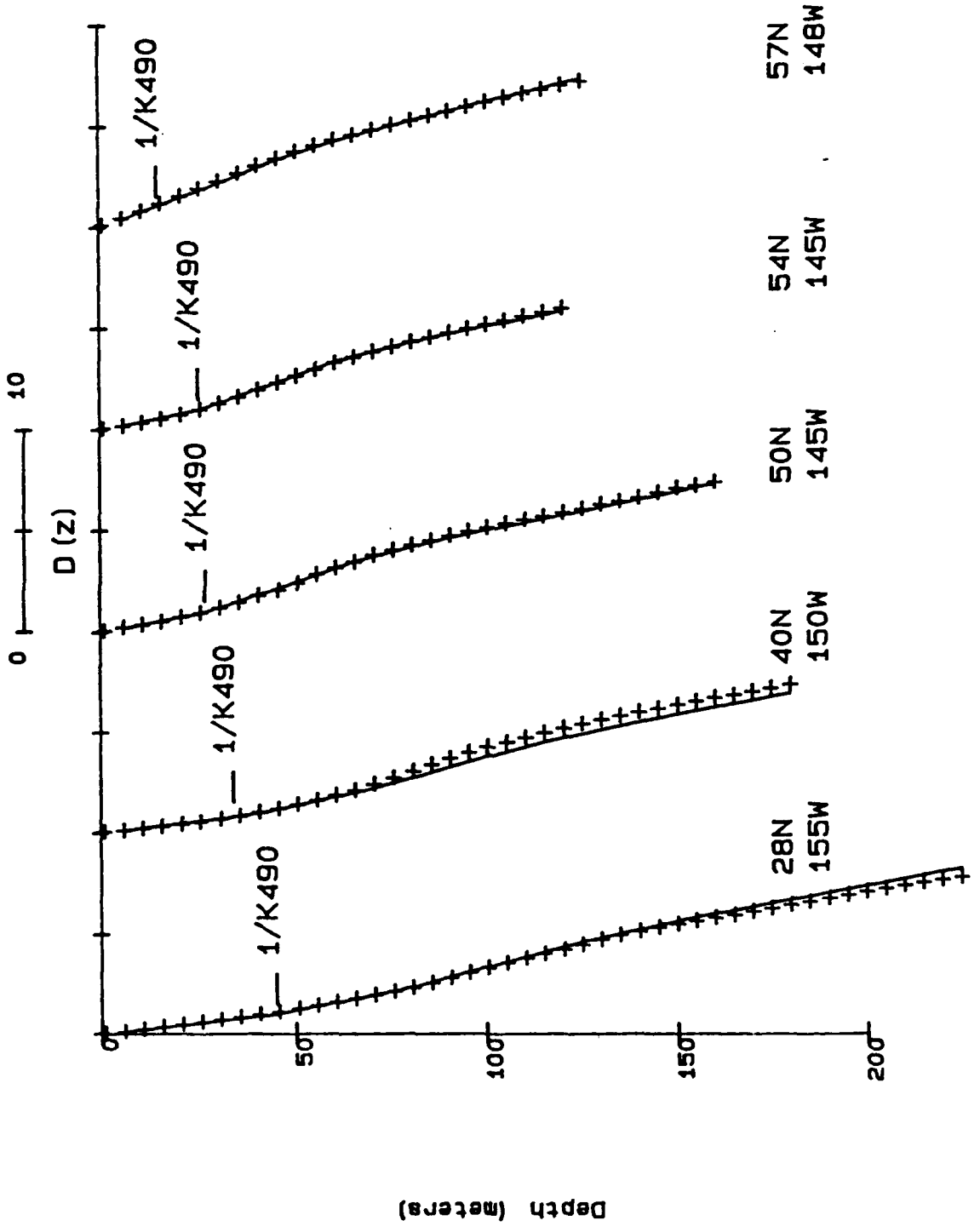
1/K490
57N
148W
54N
145W
50N
145W
40N
150W
28N
155W
D (z)
0
10
0
50
100
150
200
Depth (meters)

FIGURE 12b

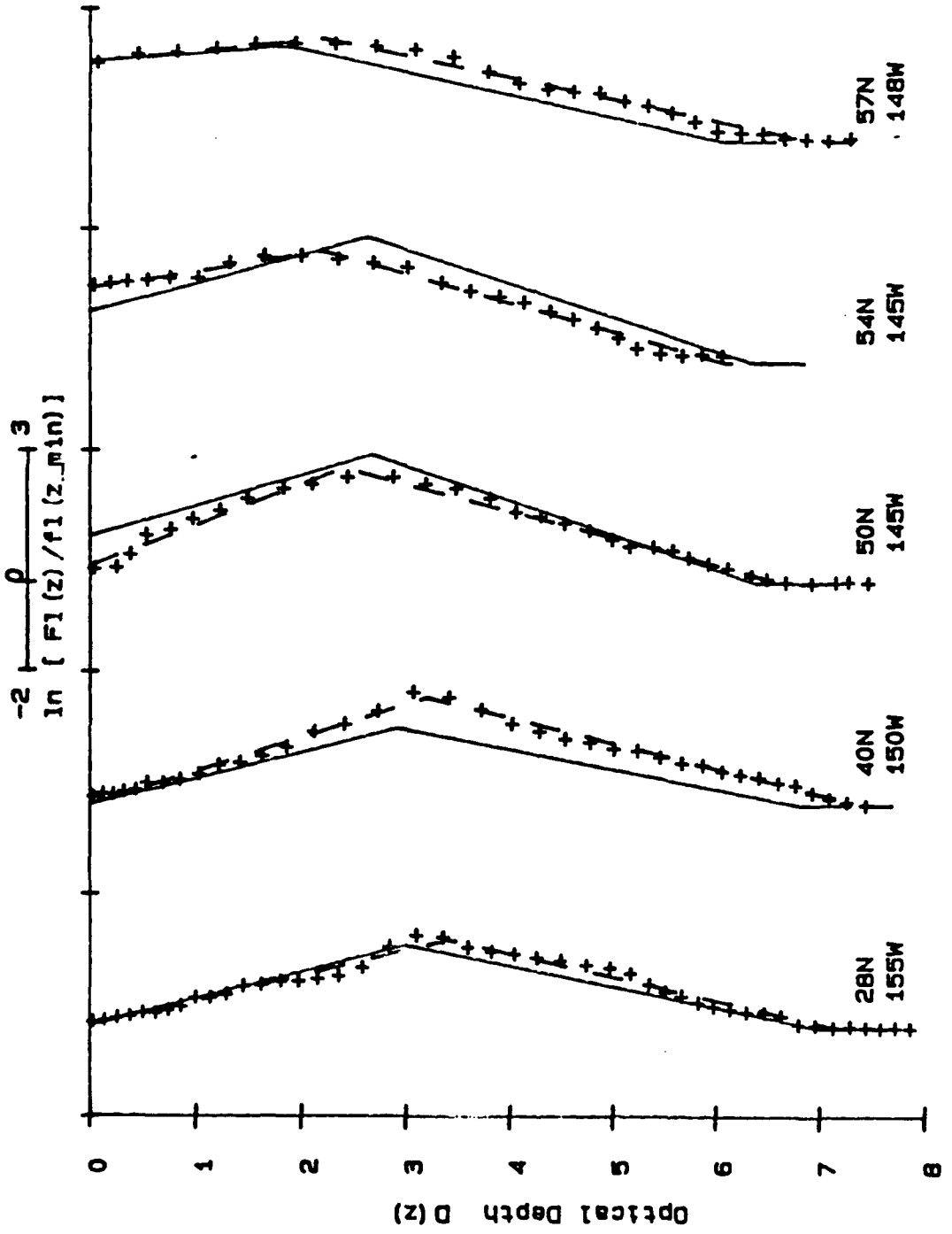
57N 148W
54N 145W
50N 145W
40N 150W
28N 155W
-2
0
3
ln [F1(z) /f1(z_min)]
0
1
2
3
4
5
6
7
8
Optical Depth D(z)

FIGURE 12c

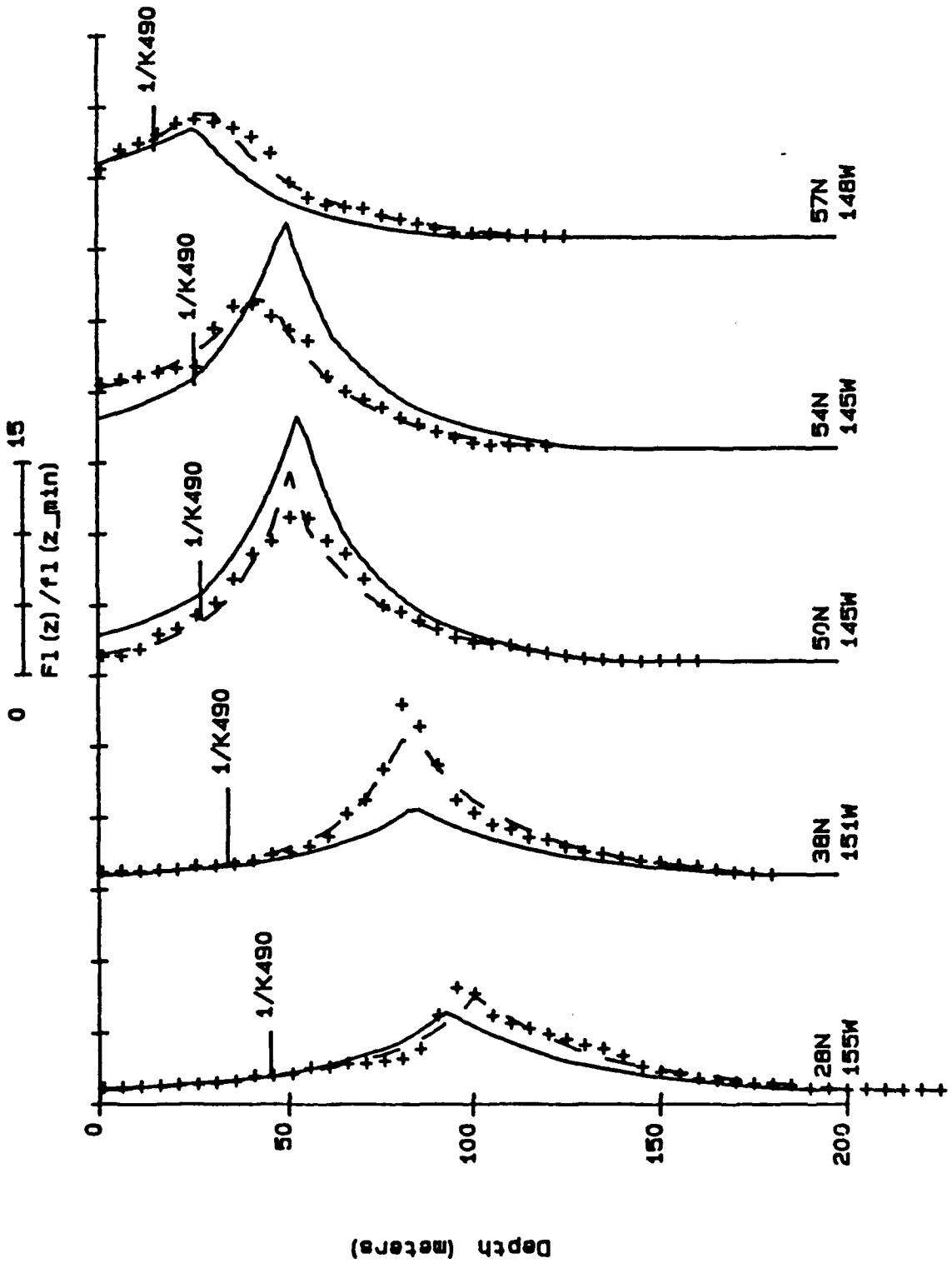
1/K490
57N 148W
54N 145W
50N 145W
38N 151W
28N 155W
0
15
F1(z)/f1(z_min)
0
50
100
150
200
Depth (meters)

FIGURE 13a

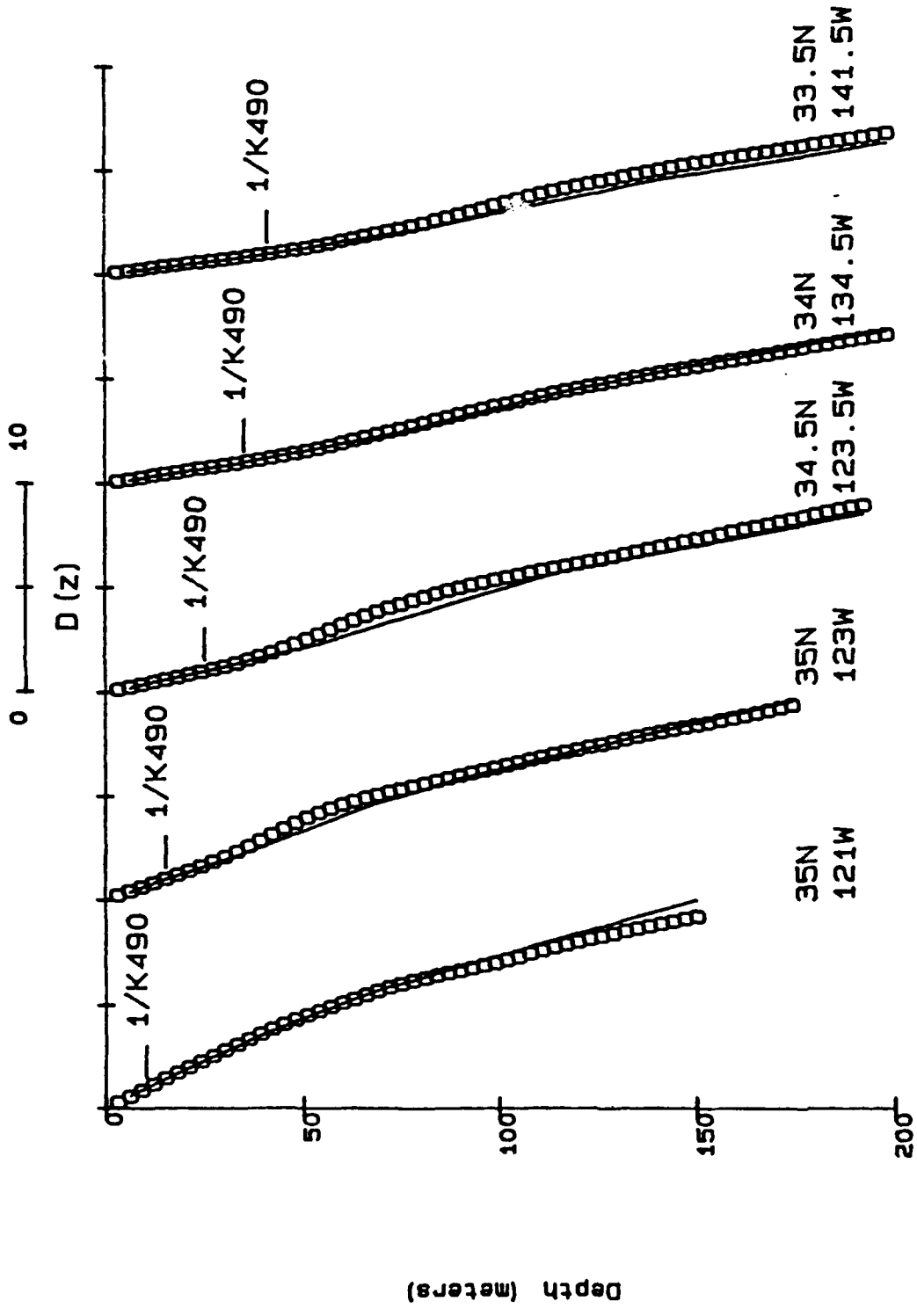
33.5N
141.5W
34N
134.5W
34.5N
123.5W
35N
123W
35N
121W
1/K490
1/K490
1/K490
1/K490
1/K490
0
10
D (z)
0
50
100
150
200
Depth (meters)

FIGURE 13b

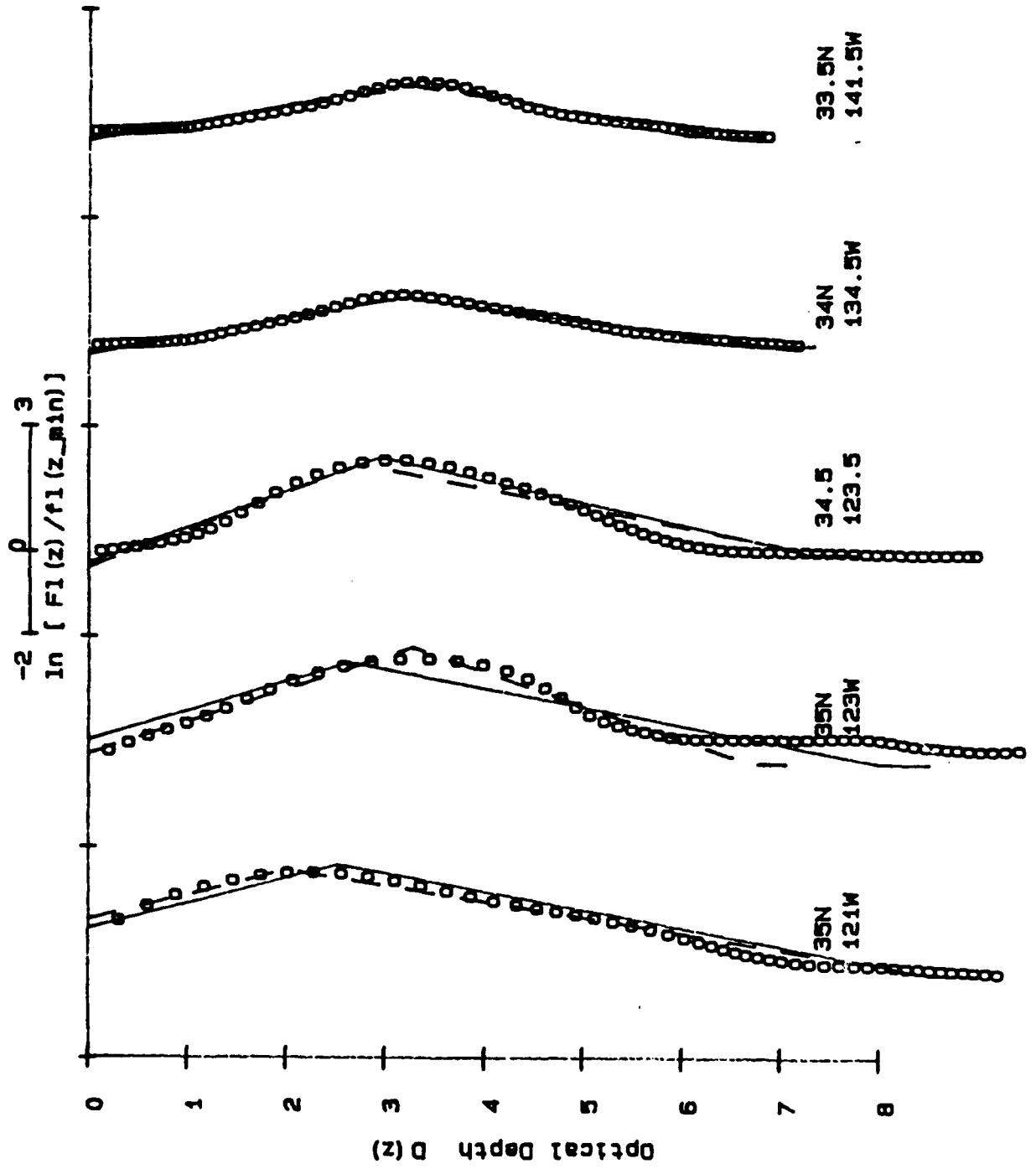
33.5N
141.5W
34N
134.5W
34.5
123.5
35N
123W
35N
121W
-2
0
3
ln [F1(z)/F1(z_min)]
0
1
2
3
4
5
6
7
8
Optical Depth D(z)

FIGURE 13c

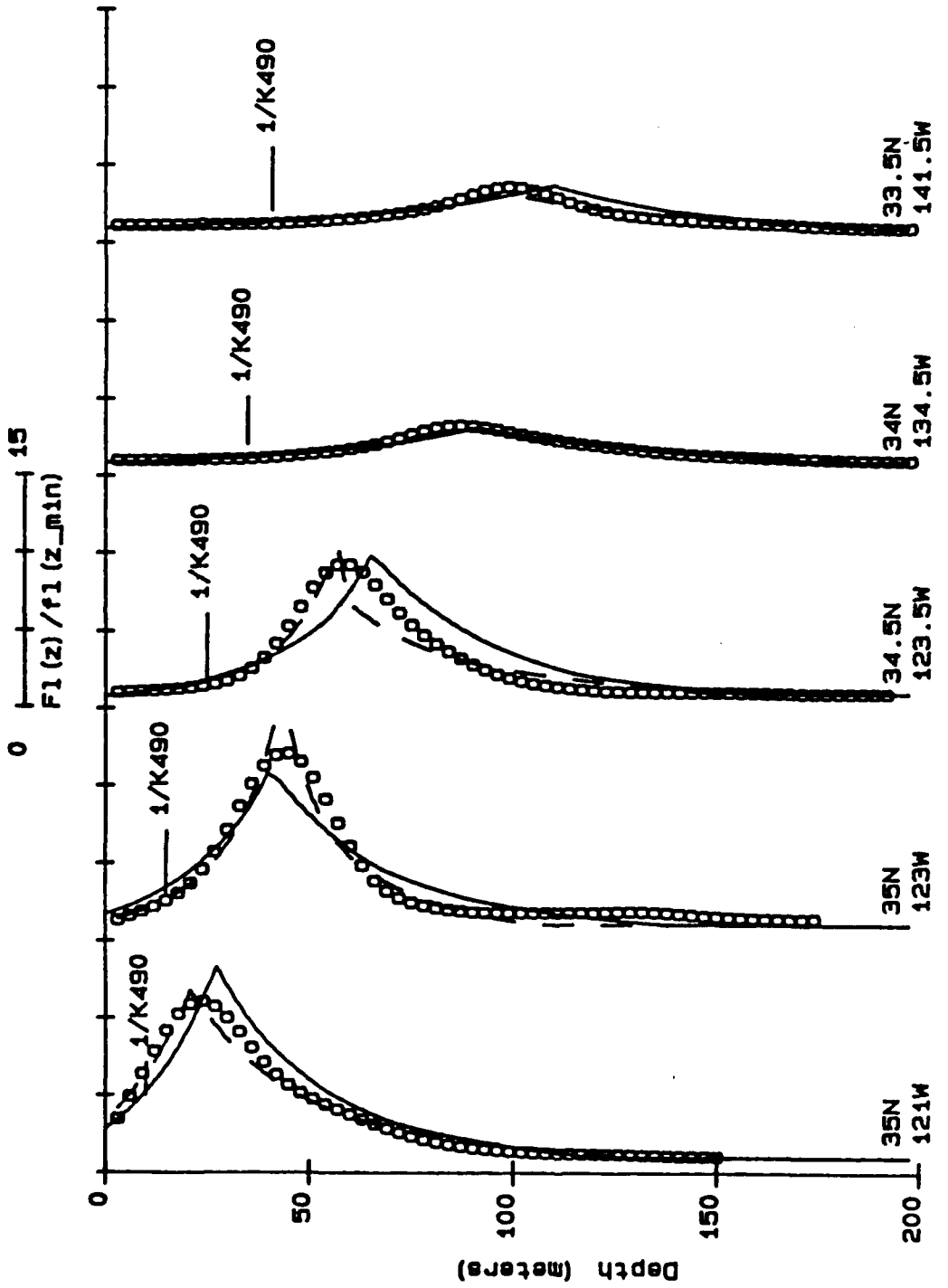
0
15
F1(z)/f1(z_min)
1/K490
1/K490
1/K490
1/K490
1/K490
33.5N
141.5W
34N
134.5W
34.5N
123.5W
35N
123W
35N
121W
0
50
100
150
200
Depth (meters)

FIGURE 14a

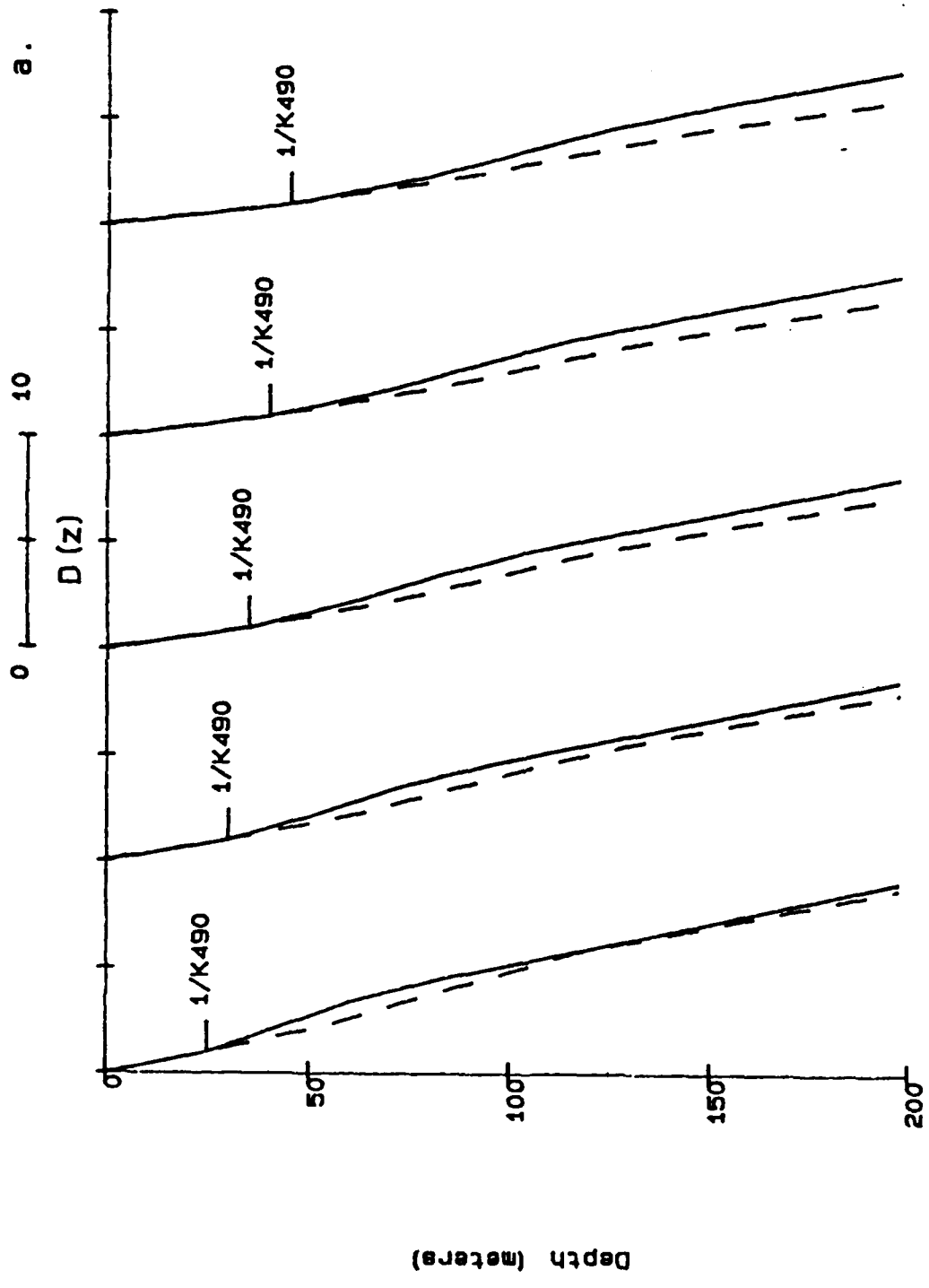
a.
0
10
D (z)
1/K490
1/K490
1/K490
1/K490
1/K490
0
50
100
150
200
Depth (meters)

FIGURE 14b

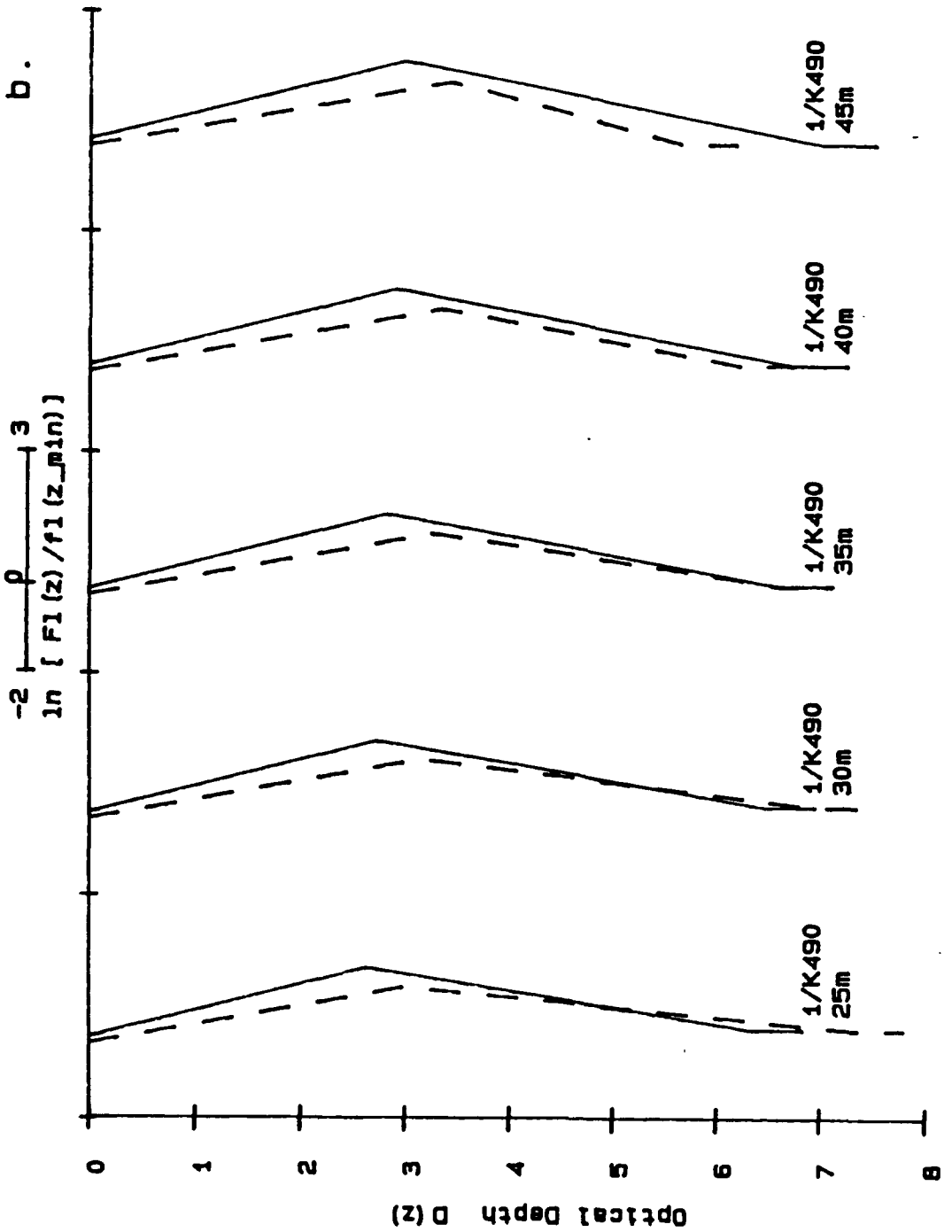
b.
-2
0
3
ln [F1(z) / f1(z_min)]
1/K490 45m
1/K490 40m
1/K490 35m
1/K490 30m
1/K490 25m
0
1
2
3
4
5
6
7
8
Optical Depth D(z)

FIGURE 14c

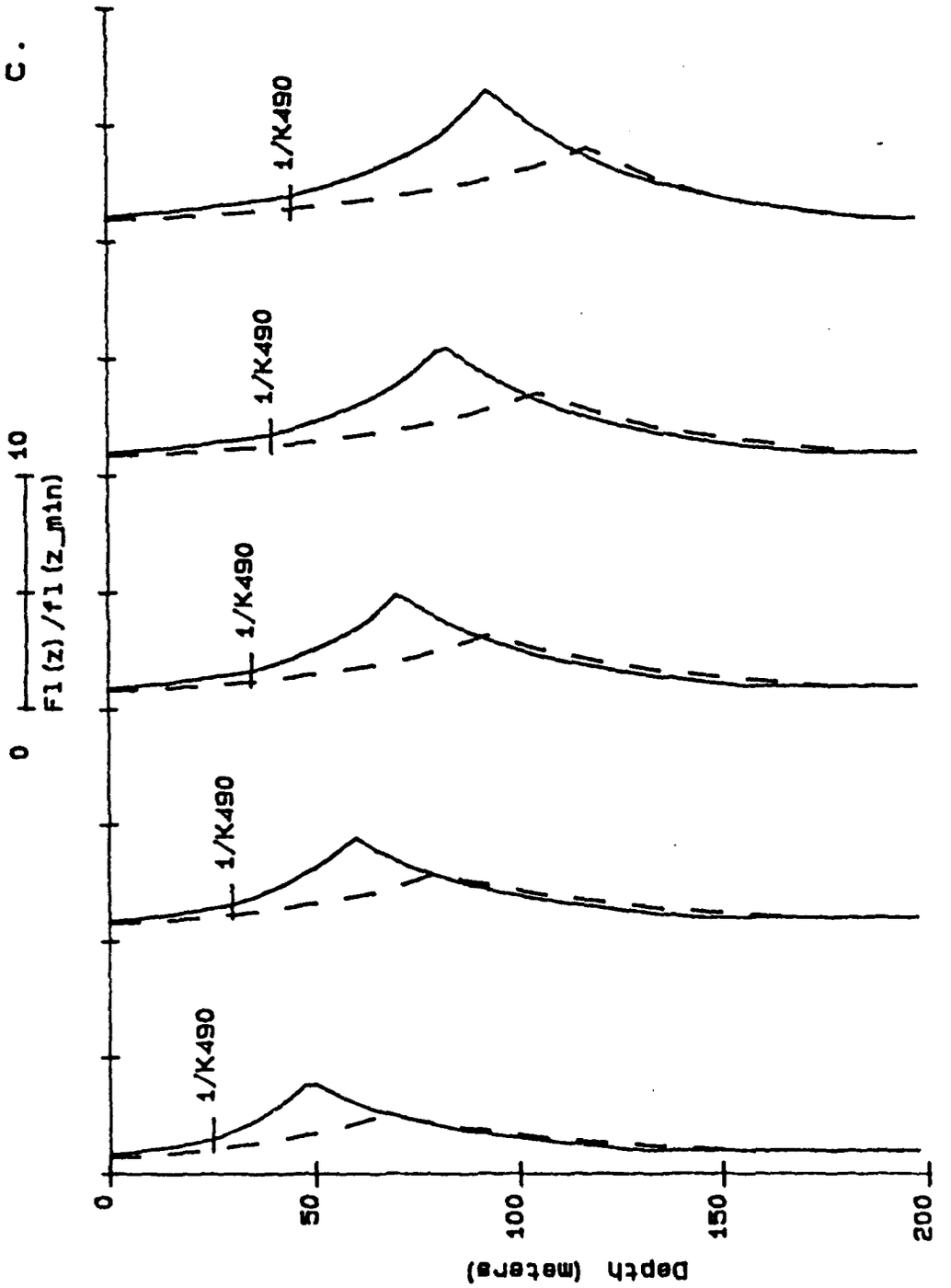
C.
1/K490
1/K490
1/K490
1/K490
1/K490
0
10
F1(z)/f1(z_min)
0
50
100
150
200
Depth (meters)

FIGURE 15.

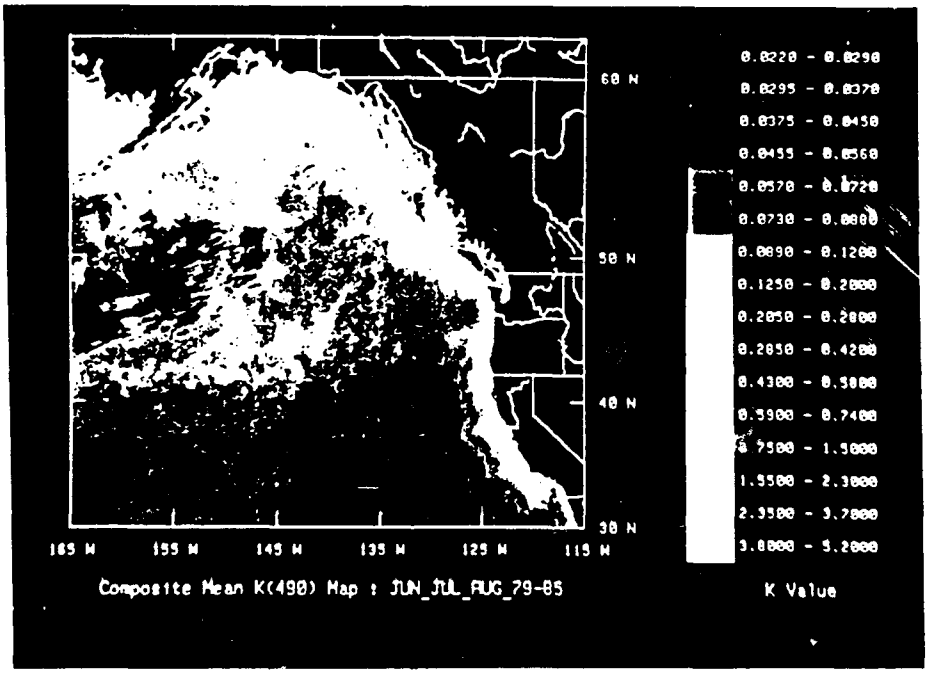
60 N
50 N
40 N
30 N
165 W
155 W
145 W
135 W
125 W
115 W
Composite Mean K(490) Map : JUN_JUL_AUG_79-85
0.0220 - 0.0290
0.0295 - 0.0370
0.0375 - 0.0450
0.0455 - 0.0560
0.0570 - 0.0720
0.0730 - 0.0880
0.0890 - 0.1200
0.1250 - 0.2000
0.2050 - 0.2800
0.2850 - 0.4200
0.4300 - 0.5800
0.5900 - 0.7400
0.7500 - 1.5000
1.5500 - 2.3000
2.3500 - 3.7000
3.8000 - 5.2000
K Value

FIGURE 16

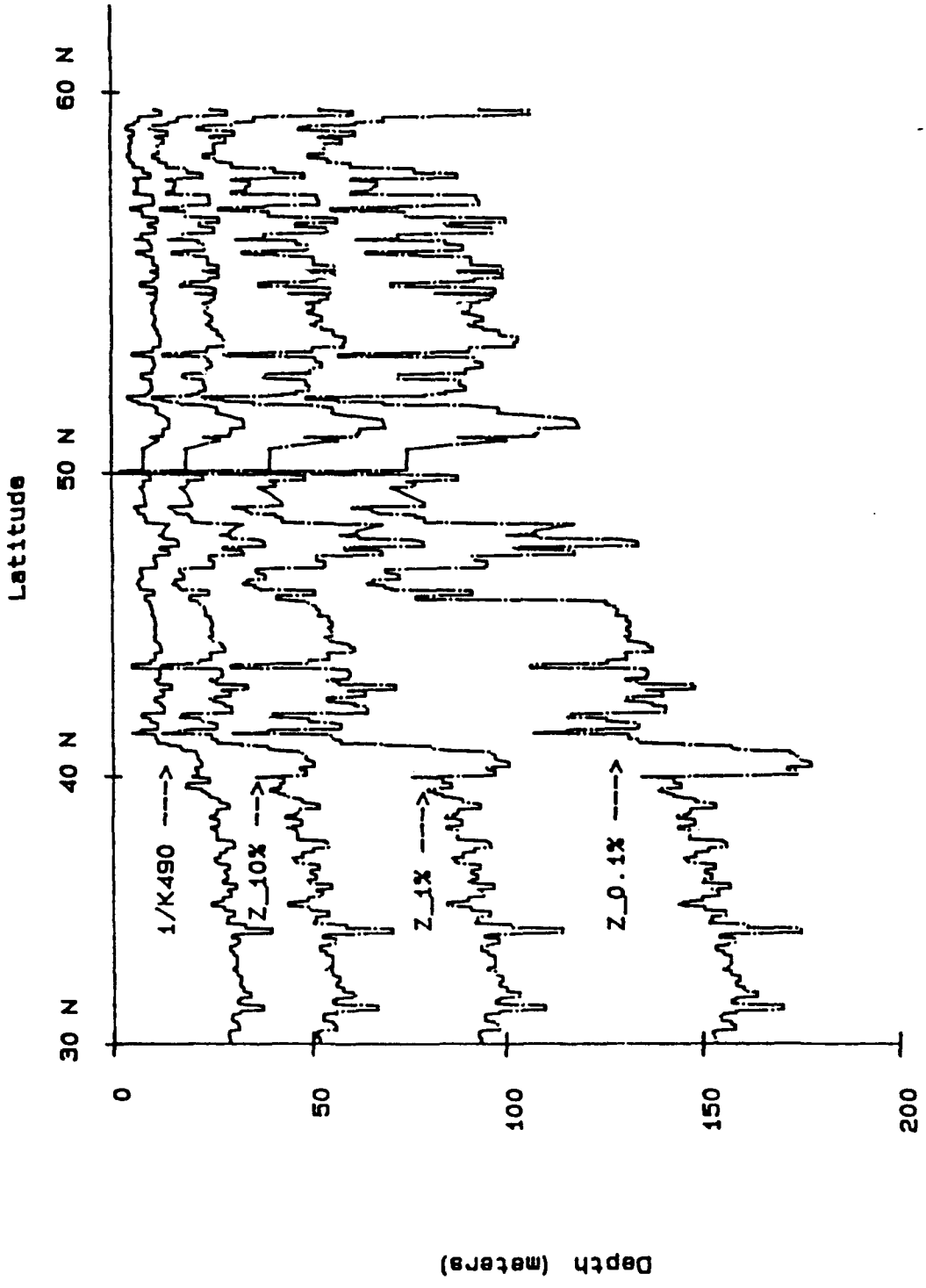
Latitude
60 N
50 N
40 N
30 N
1/K490 --->
Z_10% --->
Z_1% --->
Z_0.1% --->
0
50
100
150
200
Depth (meters)

FIGURE 1

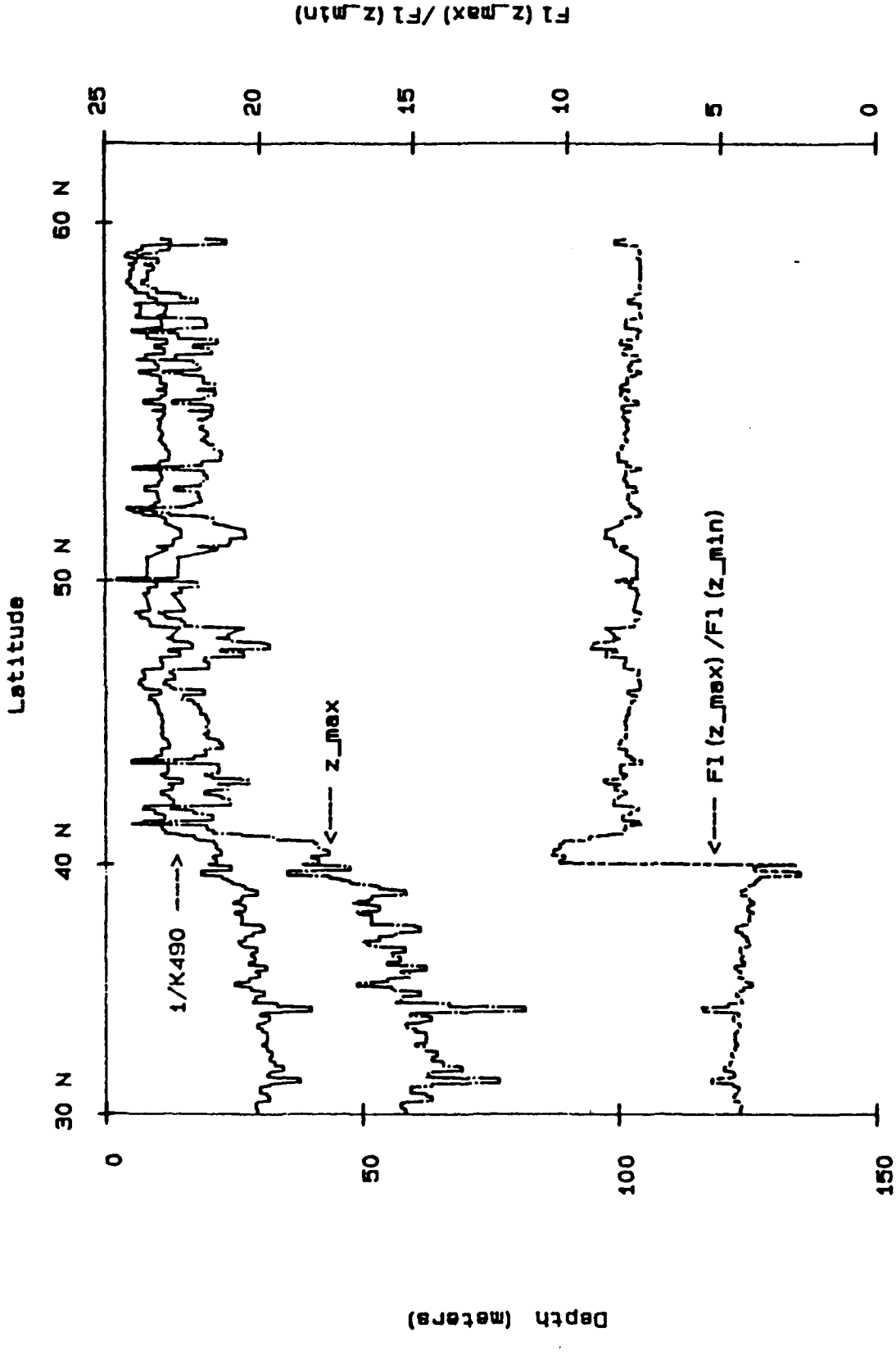
F1 (z_max) /F1 (z_min)
25
20
15
10
5
0
60 N
50 N
40 N
30 N
Latitude
1/K490 ---->
z_max
<---- F1 (z_max) /F1 (z_min)
0
50
100
150
Depth (meters)